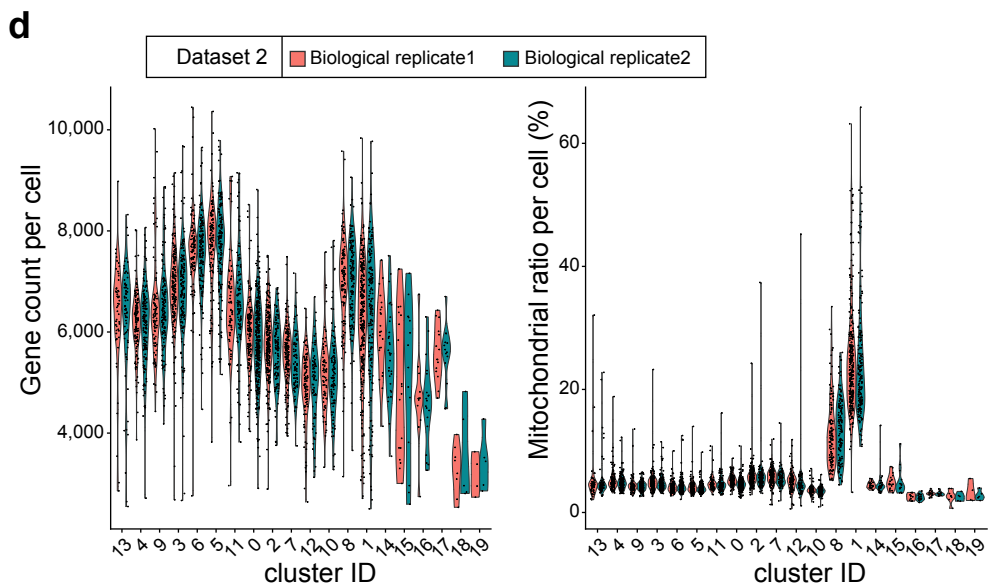
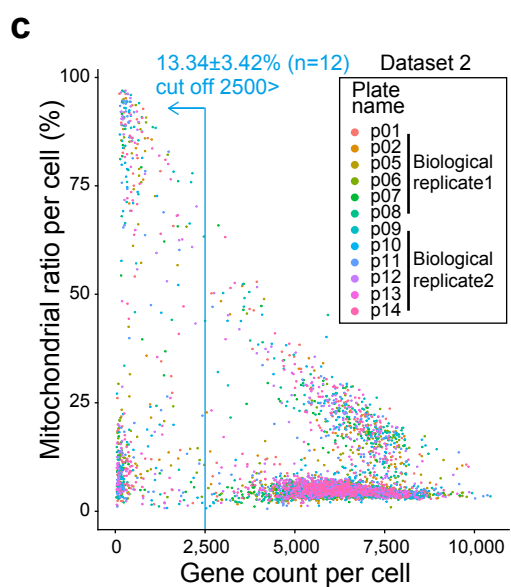
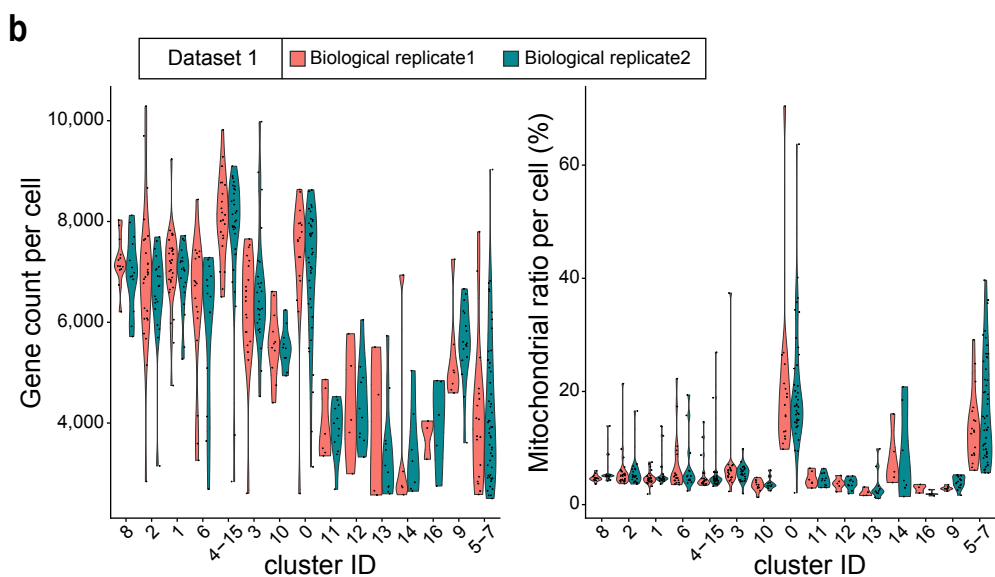
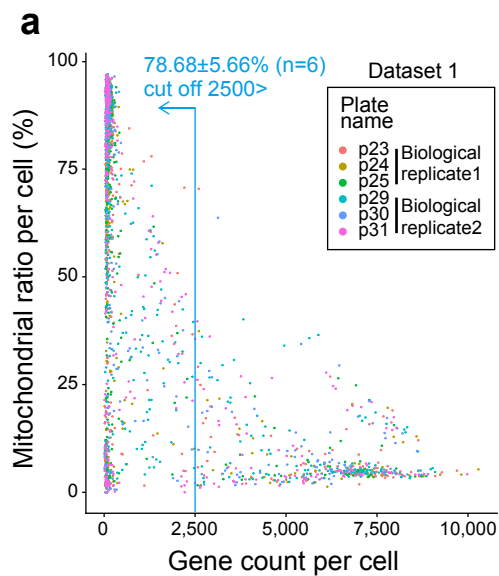


Supplementary Fig. 1 Single cell sorting of gastric cells. Related to Fig. 1

a Single cell sorting of dataset 1. After the removal of small events (left, R1), dead cells were removed based on PI staining (middle, R7), and the cells in the singlet gate (right, R1&R7&R9) were sorted to 384 well plates.

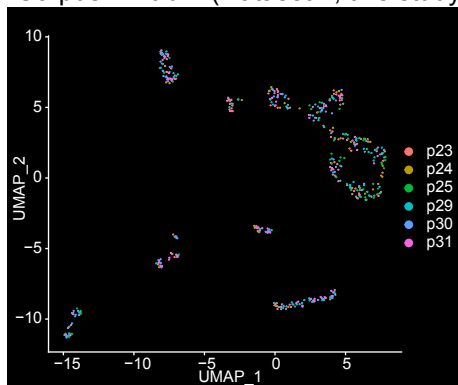
b Single cell sorting of dataset 2. After the removal of dead cells by TO-PRO-3 staining (left, R9), the cells with nuclei were selected based on Hoechst 33342 (middle, R7), and cells in the singlet gate (right, R9&R7&R5) were sorted to 384 well plates.

c Phase contrast images of dissociated gastric cells used for single cell sorting in dataset 2. Before cell sorting (left), the cell sample contains debris (white arrowheads). The singlet gate R9&R7&R5 in (b) contains neither debris nor cell aggregates (middle). The aggregate gate R9&R7&R8 in (b) contains cell doublets, triplets (black arrowheads, right), and some larger cells. Scale bar, 50 μm . These images are representative of three images from one single cell sorting experiment.

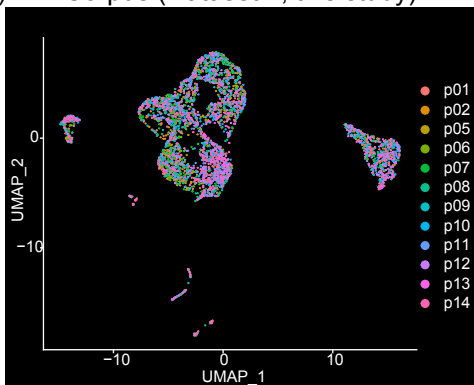


e

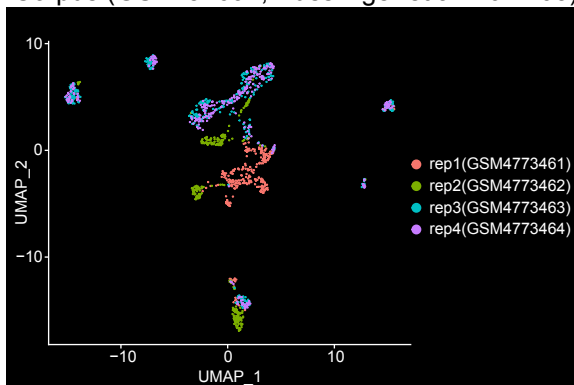
Corpus+Antrum (Dataset 1, this study)



Corpus (Dataset 2, this study)



Corpus (GSE157694, Busslinger et al. 2021/03)



Supplementary Fig. 2 Quality control of single-cell RNA-seq data. Related to Fig. 1

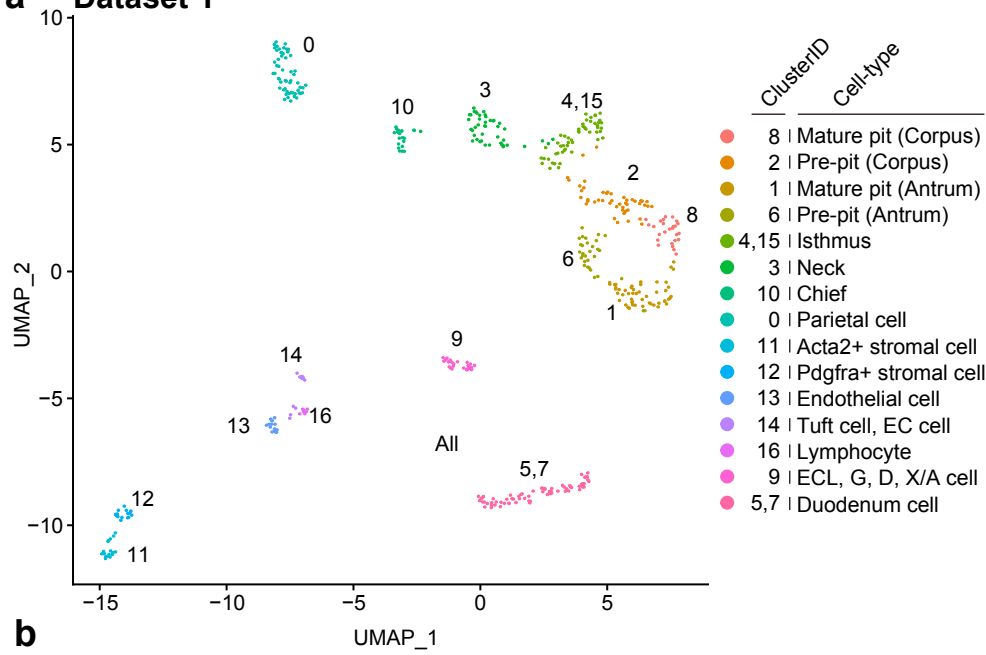
a Scatter plot showing gene count and mitochondrial ratio of all sequenced cells in dataset 1. The cells are colored by plate ID. The cells with less than 2,500 gene counts were removed as low-quality cells.

b Violin plots showing gene count and mitochondrial ratio of the cells that passed quality control in each cluster. Two biological replicates prepared by different operators were shown in red and green.

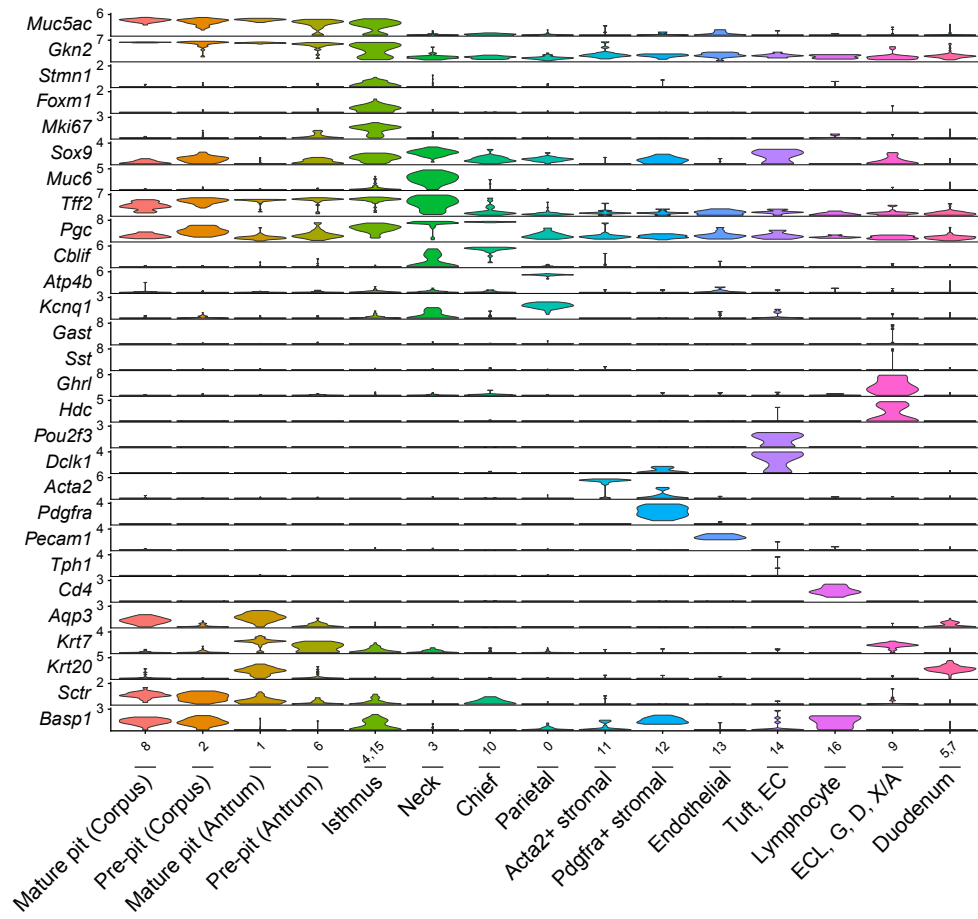
c Scatter plot showing gene count and mitochondrial ratio of all sequenced cells in dataset 2. The cells are colored by plate ID. The cells with less than 2,500 gene counts were removed as low-quality cells.

d Violin plots showing gene count and mitochondrial ratio of the cells that passed quality control in each cluster. Two biological replicates prepared by different operators were shown in red and green. **e** UMAP of gastric cells in dataset 1 (left, our study), dataset 2 (middle, our study), and the previously published dataset (right, GSE157694). In our study, the cells were colored by plate ID. In the previously published data, the cells were colored by plates. Note that, in our study, the cells from six plates (dataset 1, two biological replicates) or twelve plates (dataset 2, two biological replicates) were clustered together, suggesting that our data is not affected by technical noise.

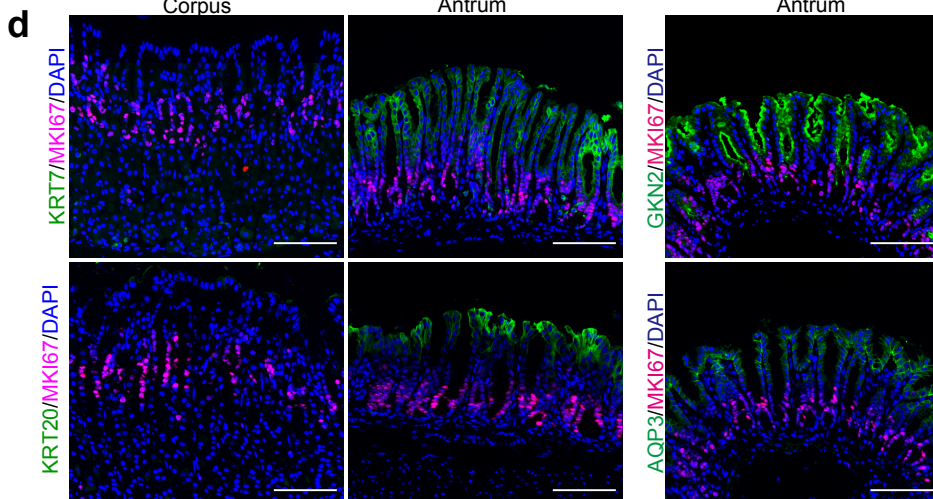
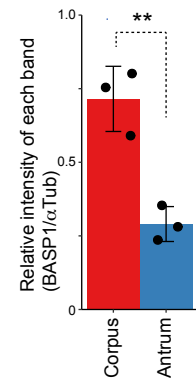
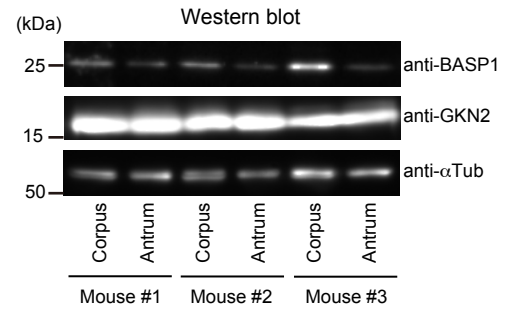
a Dataset 1



b



c



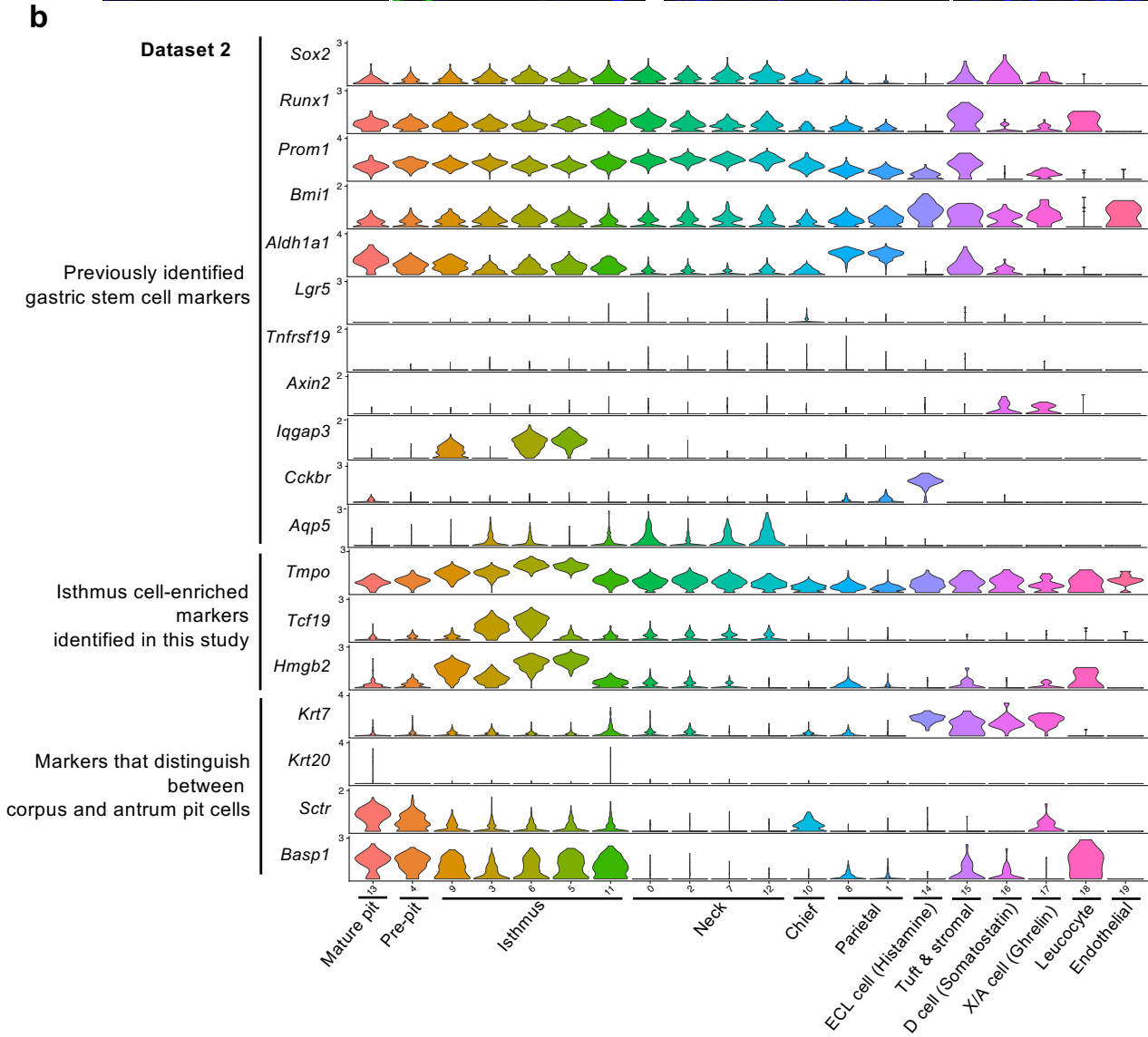
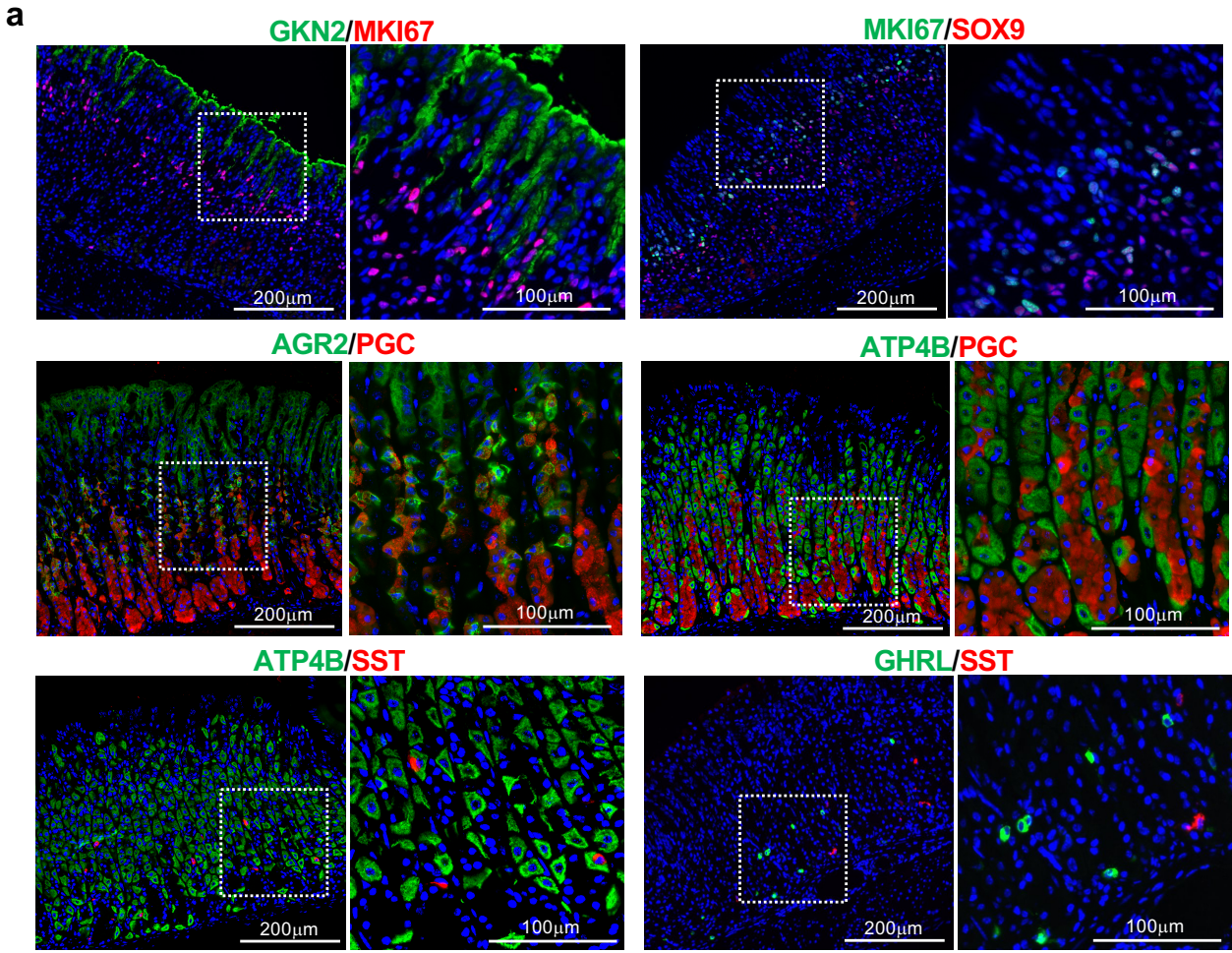
Supplementary Fig. 3. Single-cell analysis of corpus and antrum gastric units (dataset 1).

a UMAP visualization of the cells isolated from the corpus and antrum gastric units (dataset 1). Cells are colored according to the clustering results.

b Violin plots of dataset 1 showing the expression of known marker genes in each cluster.

c Western blotting showing the expression of BASP1 (top), GKN2 (middle), and α -Tubulin (bottom) in corpus and antrum glands isolated from three different mice. Data are presented as mean relative expression \pm SD. Significance was calculated by two-tailed Student's t-tests ($**p = 0.0042$). Source data are provided as a Source Data file.

d Immunofluorescence staining of adult mouse corpus and antrum tissue with KRT7 (green), KRT20 (green), MKI67 (red), and DAPI (blue). Scale bar, 100 μ m. The images of KRT20, GKN2, and AQP3 staining are representative of three independent experiments. The images of KRT7 staining are representative of two independent experiments.



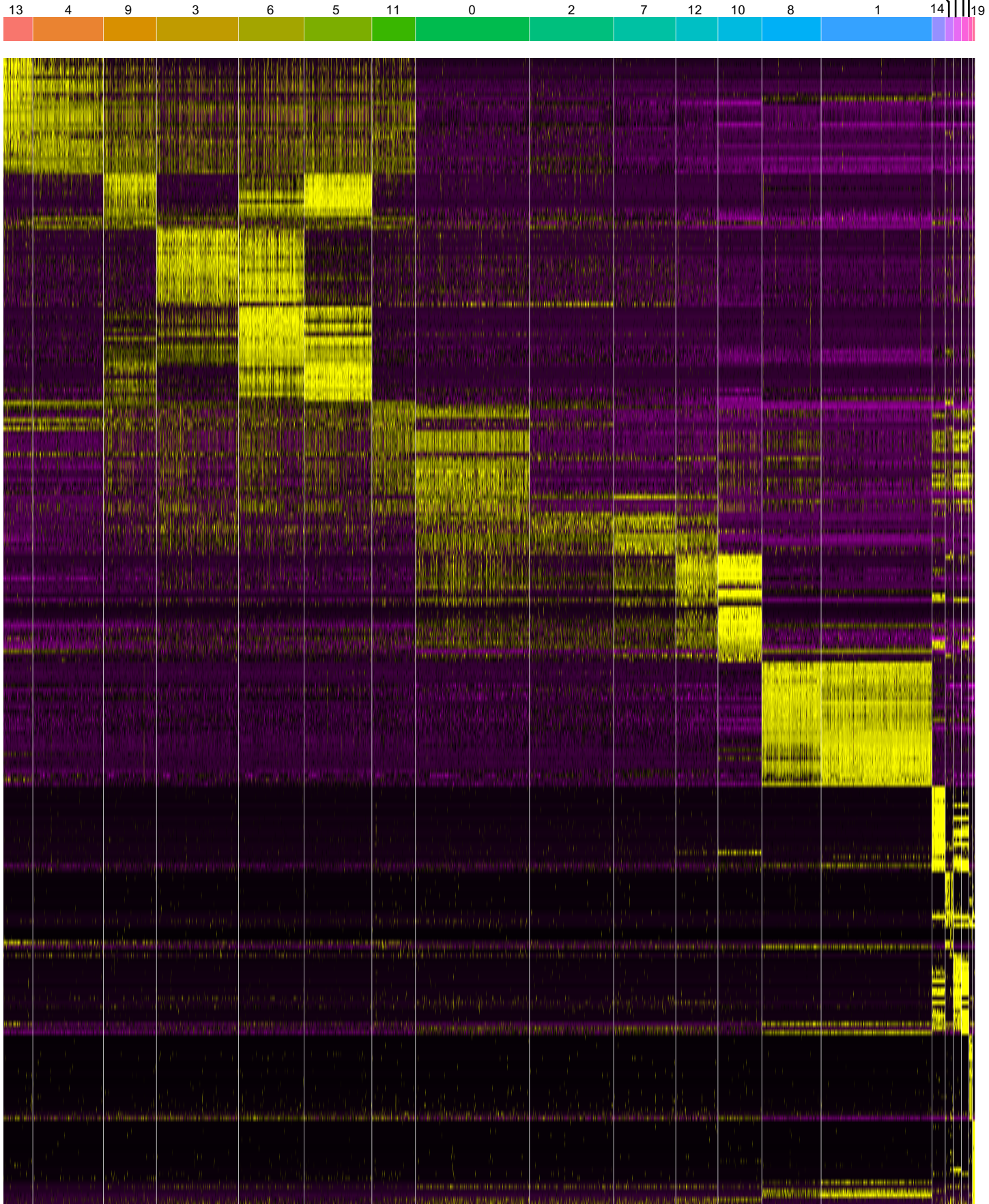
Supplementary Fig. 4. Expression pattern of various gastric epithelial cell markers in adult mouse corpus tissue. Related to Fig. 1.

a Immunofluorescence staining of the corpus tissues with cell type-specific markers. High magnification images of the dotted squares are shown on the right side. All images are representative of two independent experiments.

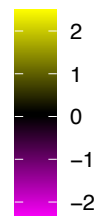
b Violin plots of dataset 2 showing the expression of previously identified gastric stem cell markers, isthmus progenitor cell-enriched markers identified in this study, and the markers that distinguish between corpus and antrum pit cells.

Dataset 2

15 16 17 18 19

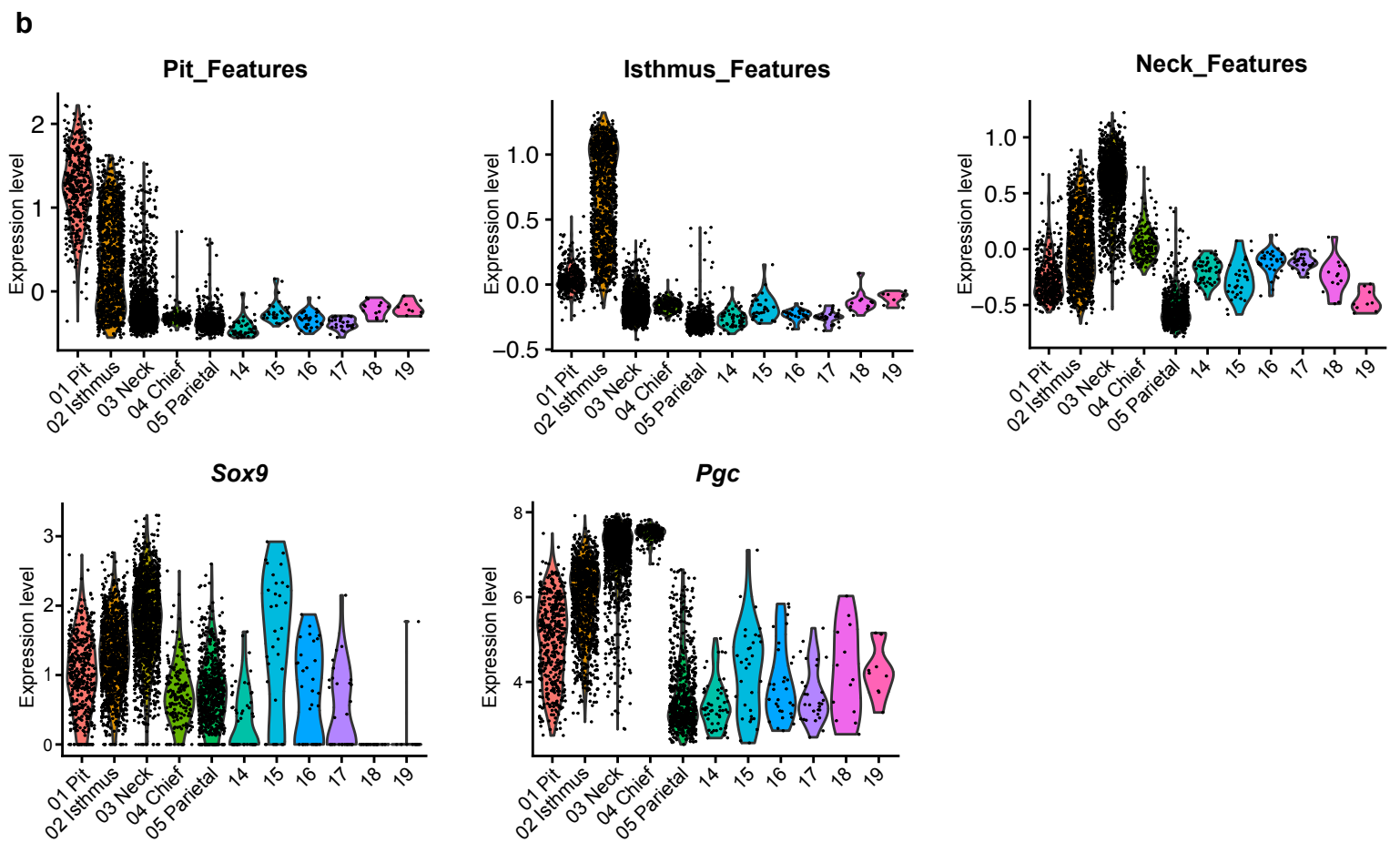
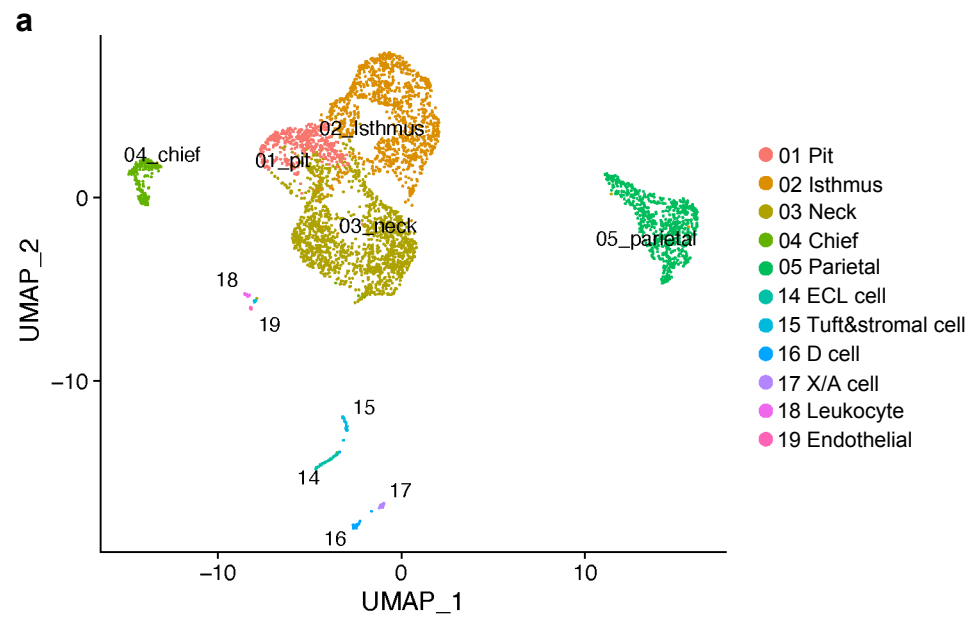


Expression



Supplementary Fig. 5. Cell type-specific markers identified in dataset 2. Related to Fig. 1

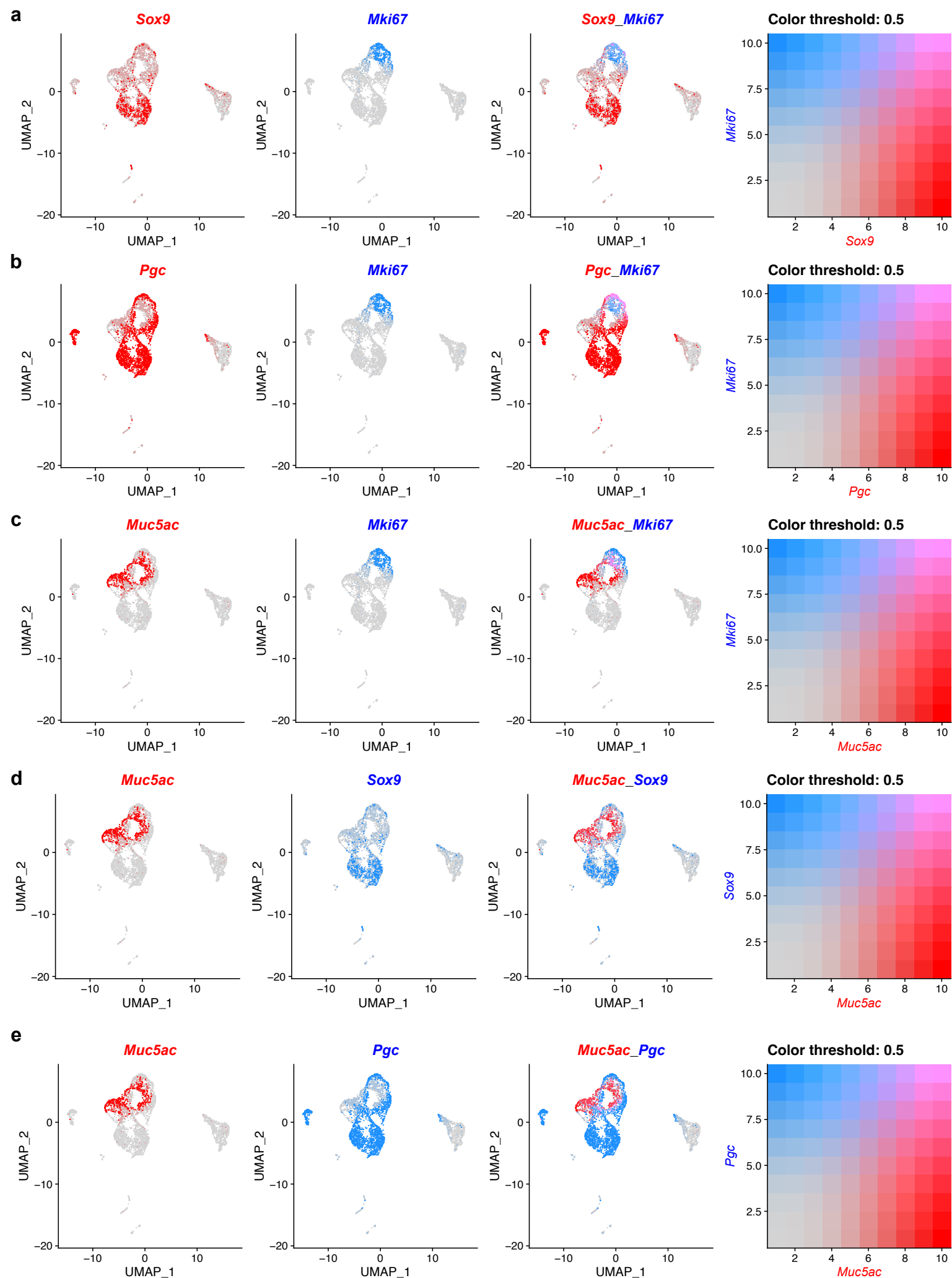
Heatmap showing the expression of cell type-specific marker genes in individual cells. Differentially expressed genes with LogFC > 0.75 were used to generate this heatmap.



Supplementary Fig. 6. Expression of Sox9 and Pgc in combined clusters. Related to Fig. 1

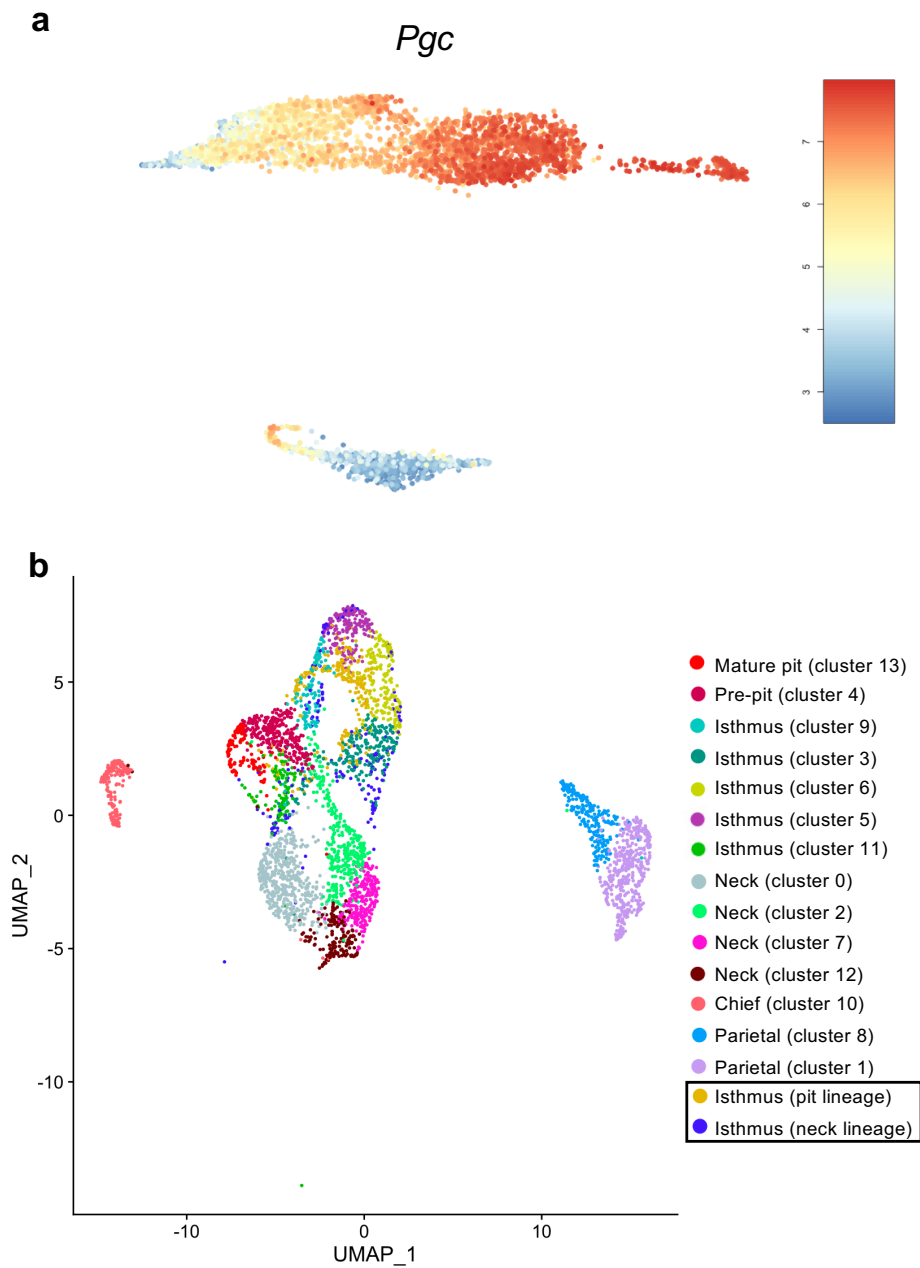
a UMAP visualization of the cells identified in dataset 2. The multiple clusters of same cell types were combined into one cluster.

b Top: violin plots showing the expression of top 50 genes enriched in pit cells (Pit_Features), in isthmus progenitor cells (Isthmus_Features), and in neck cells (Neck_Features). Bottom: violin plots showing the expression of Sox9 and Pgc.



Supplementary Fig. 7. Comparison of the expression profiles of *Muc5ac*, *Mki67*, *Sox9*, and *Pgc*. Related to Fig. 1

UMAP of gastric cells colored by the expression level of *Sox9* and *Mki67* (a), *Pgc* and *Mki67* (b), *Muc5ac* and *Mki67* (c), *Muc5ac* and *Sox9* (d), and *Muc5ac* and *Pgc* (e).

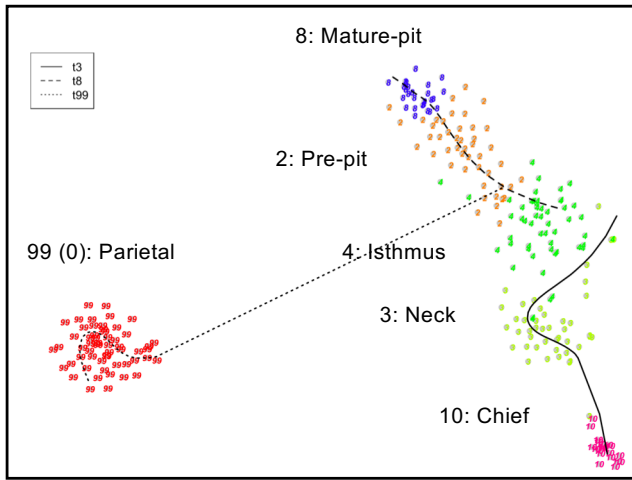


Supplementary Fig. 8. Pseudotime analysis of major corpus epithelial cells identified in dataset 2. Related to Fig. 2.

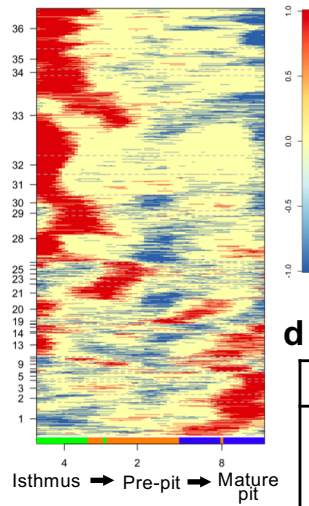
a The expression level of *Pgc* along differentiation trajectories (dataset 2).

b UMAP visualization of isthmus progenitor cells identified in pit cell or neck cell lineage by FateID analysis. Note that isthmus progenitor cells used for pit cell (yellow) or neck cell (blue) lineage by FateID were merged with isthmus progenitor cells with high pit cell feature or high neck cell feature identified in Fig. 1f, supporting the reliability of FateID analysis.

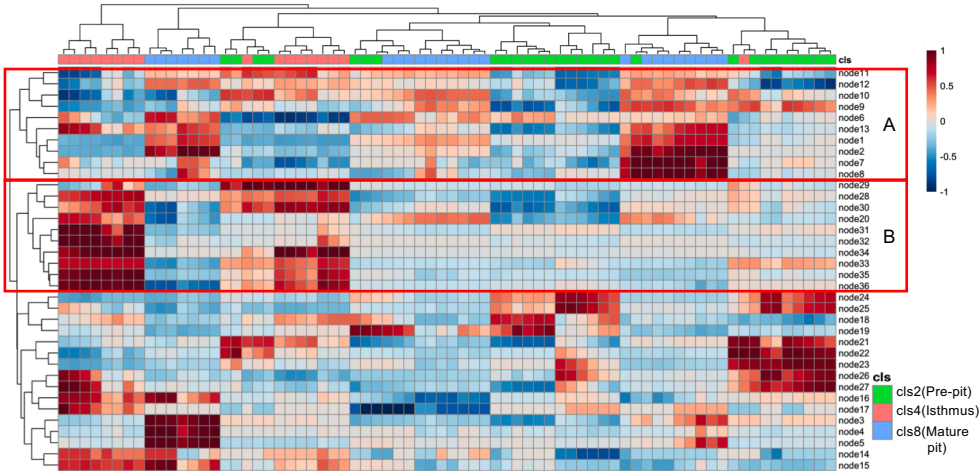
a Dataset 1



b



c



d

	Marker gene	Expression pattern	TF
A	<i>Gkn2</i> <i>Gkn1</i> <i>Muc5ac</i>	Node 1 	<i>Klf4</i> <i>Stat1</i> <i>Pparg</i> <i>Fosl2</i> <i>Foxa3</i> <i>Foxq1</i> <i>Elf3</i> <i>Stat2</i> <i>Elf4</i> <i>Tcf23</i>
		Node34 	<i>Cenpa</i> <i>Fos</i> <i>Dnmt1</i> <i>Tfdp1</i> <i>Egr1</i> <i>Junb</i> <i>Foxm1</i> <i>Cebpb</i> <i>Jun</i> <i>Mxd3</i>

e

Group A (Upregulation)	
Pathways	
Term	adj. p-value
EGFR1 signaling pathway	9.4047E-05
Triacylglyceride synthesis	0.00054875
Alpha 6 beta 4 integrin signaling pathway	0.0007502
Sphingolipid metabolism overview	0.00614722
Mitochondrial long chain fatty acid beta-oxidation	0.00657058
Fatty acid beta-oxidation	0.00845411
Sphingolipid metabolism (integrated pathway)	0.00926181
Eicosanoid metabolism via cyclooxygenases (COX)	0.01087412
Alzheimer's disease	0.01483459
IL-3 signaling pathway	0.01719836
GO (Biological Pathway)	
Term	adj. p-value
organonitrogen compound biosynthetic process	1.02E-05
sphingolipid biosynthetic process	2.67E-05
membrane lipid biosynthetic process	3.44E-05
membrane organization	4.40E-05
multivesicular body organization	2.58E-04

f

Group B (Downregulation)	
Pathways	
Term	adj. p-value
mRNA processing	9.86E-39
TNF-alpha NF-kB signaling pathway	1.47E-14
DNA replication	9.37E-14
Cytoplasmic ribosomal proteins	2.13E-12
G1 to S cell cycle control	1.85E-10
Proteasome degradation	3.01E-09
Electron transport chain	1.70E-08
Eukaryotic transcription initiation	2.43E-08
Estrogen signaling	4.2702E-06
TCA cycle	0.00020323
GO (Biological Pathway)	
Term	adj. p-value
mRNA processing	3.38E-67
mRNA splicing, via spliceosome	2.62E-65
RNA splicing, via transesterification reactions with bulged adenosine as nucleophile	3.08E-61
gene expression	6.26E-57
cellular macromolecule biosynthetic process	4.04E-52

Supplementary Fig. 9. Characterization of the pit cell differentiation process in dataset 1. Related to Fig.2.

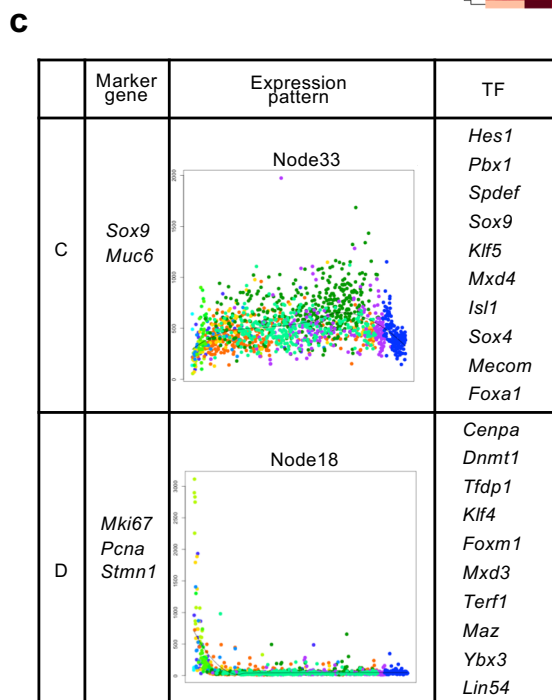
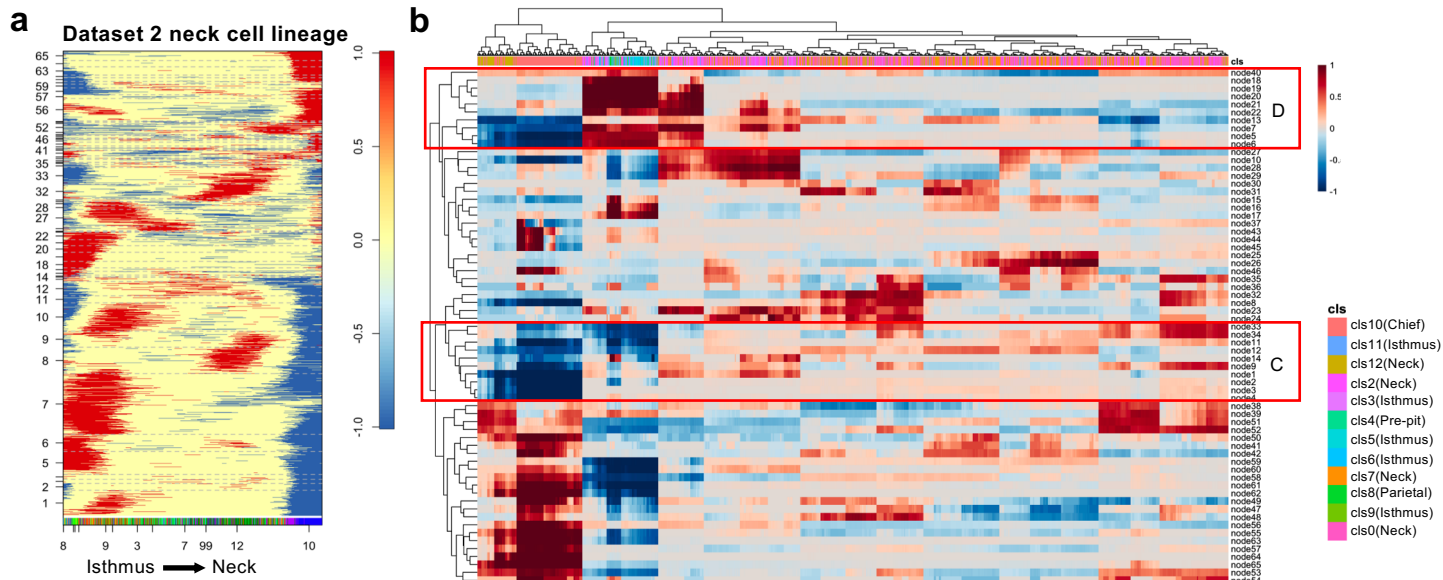
a Pseudotemporal ordering of major corpus epithelial cells identified in dataset 1. Principal curves are shown for mature pit cells (t8, heavy dotted line), neck cells (t3, solid line), and parietal cells (t99, fine dotted line).

b Self-organizing map of binarized pseudotemporal expression profiles along the pit cell differentiation trajectory. The x-axis indicates the cells involved in the pit cell lineage that are colored according to cell types and the y-axis indicates the nodes.

c Hierarchical clustering of co-expression nodes in (b). The nodes in group A and B show upregulation and downregulation patterns of the genes in the pit cell differentiation trajectory, respectively. The x-axis indicates the cells involved in the pit cell lineage that are colored according to cell types and the y-axis indicates the nodes. The x-axis in (c) is not same as that of (b) due to the new hierarchical clustering of the cells. The colors for each cell type are shown on the right bottom corner.

d Characteristics of group A and B defined in (c). Previously reported marker genes in each group are shown. Average pseudotemporal expression profile of the representative node is shown in gray line. The x-axis indicates pseudotime from isthmus progenitor cells to pit cells and the y-axis indicates expression level. Colors of each dot represent cell types, which corresponds to colors used in (a). Among the TFs involved in group A and B, the top 10 TFs specifically expressed in pit cells and isthmus progenitor cells ($\text{LogFC} > 0.25$) are shown, respectively.

e and f Characterization of the pseudotime-dependent genes included in group A (e) and group B (f). Upper panel, pathway enrichment analysis of the pseudotime-dependent genes. The top ten pathways with significant enrichment (adjusted p-value < 0.05) are listed. Lower panel, GO analysis of the pseudotime-dependent genes. The top five terms with significant enrichment (adjusted p-value < 0.05) are listed. Adjusted p-value was determined using one-tailed Fisher's exact test with g:SCS method in g:Profiler³⁶ (pathways) and Fisher's exact test with Benjamini-Hochberg adjustment in Enrichr³⁷ (GO).



d

Group C (Upregulation)	
Pathways	
Term	adj. p-value
Kit receptor signaling pathway	0.0029467
Fatty acid biosynthesis	0.00316366
IL-7 signaling pathway	0.00600176
IL-5 signaling pathway	0.011178
IL-6 signaling pathway	0.01562132
Wnt signaling pathway (NetPath)	0.03008174
GO (Cellular Component)	
Term	adj. p-value
lysosome	4.80E-08
lysosomal membrane	7.82E-05
lytic vacuole membrane	1.07E-04
lytic vacuole membrane	5.46E-04
lysosomal lumen	0.00198682

e

Group D (Downregulation)	
Pathways	
Term	adj. p-value
mRNA processing	9.04E-29
Cytoplasmic ribosomal proteins	7.10E-20
DNA replication	6.86E-15
Electron transport chain	3.33E-10
G1 to S cell cycle control	3.69E-10
Proteasome degradation	6.94E-08
TNF-alpha NF-kB signaling pathway	7.02E-07
Cholesterol biosynthesis	9.2308E-05
Mismatch repair	0.00034072
Oxidative phosphorylation	0.0007799
GO (Biological Process)	
Term	adj. p-value
cellular macromolecule biosynthetic process	1.29E-54
rRNA processing	8.83E-50
ribosome biogenesis	8.83E-50
ncRNA processing	8.27E-48
rRNA metabolic process	6.23E-43

Supplementary Fig. 10. Characterization of the neck cell differentiation process in dataset 2. Related to Fig.2.

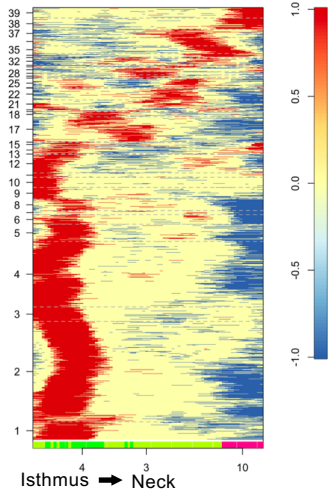
a Self-organizing map of binarized pseudotemporal expression profiles along the neck cell differentiation trajectory. The x-axis indicates the cells involved in the neck cell lineage that are colored according to cell types and the y-axis indicates the nodes.

b Hierarchical clustering of co-expression nodes in (a). The nodes in group C and D show upregulation and downregulation patterns of the genes in the neck cell differentiation trajectory, respectively. The x-axis indicates the cells involved in the neck cell lineage that are colored according to cell types and the y-axis indicates the nodes. The x-axis in (b) is not same as that of (a) because of the new hierarchical clustering of the cells. The colors for each cell type are shown on the right bottom corner.

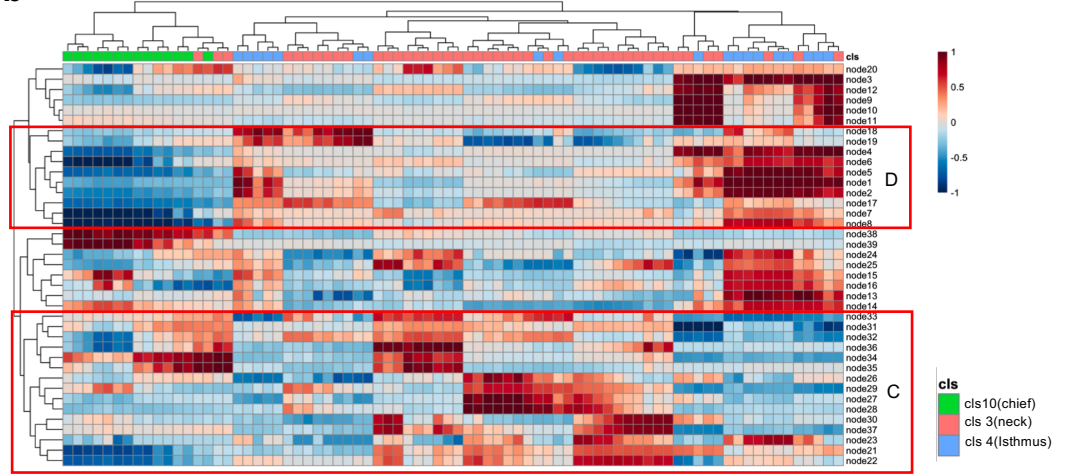
c Characteristics of group C and D identified in (b). Marker genes in each group are shown. Average pseudotemporal expression profile of the representative node is shown in black line. The x-axis indicates pseudotime from isthmus progenitor cells to neck cells and the y-axis indicates expression level. Colors in each dot represent cell types, which corresponds to colors used in Fig. 2a. Among the TFs involved in group C and D, the top 10 TFs specifically expressed in neck cells and isthmus progenitor cells ($\text{LogFC} > 0.25$) are shown here, respectively.

d and e Characterization of the pseudotime-dependent genes included in group C (d) and group D (e). Upper panel, pathway enrichment analysis of the pseudotime-dependent genes. The six pathways and the top ten pathways with significant enrichment (adjusted p -value < 0.05) are listed in group C and D, respectively. Lower panel, GO analysis of the pseudotime-dependent genes. The top five terms with significant enrichment (adjusted p -value < 0.05) are listed. Adjusted p -value was determined using one-tailed Fisher's exact test with g:SCS method in g:Profiler³⁶ (pathways) and Fisher's exact test with Benjamini-Hochberg adjustment in Enrichr³⁷ (GO).

a Dataset 1 neck cell lineage



b



C	Marker gene	Expression pattern	TF
C	Sox9 Muc6	<p>Node36</p>	<i>Hes1</i> <i>Pbx1</i> <i>Spdef</i> <i>Sox9</i> <i>Irf1</i> <i>Nfil3</i> <i>Mxd4</i> <i>Isl1</i> <i>Tcf12</i> <i>Mecom</i>
			<p>Node2</p>
D	<i>Mki67</i> <i>Pcna</i> <i>Stmn1</i>		

d

Group C (Upregulation)	
Pathways	
Term	adj. p-value
Insulin signaling	0.00133206
Focal adhesion: PI3K-Akt-mTOR signaling pathway	0.00230234
G protein signaling pathways	0.01157589
MicroRNAs in cardiomyocyte hypertrophy	0.04435215
GO (Cellular Component)	
Term	adj. p-value
lysosome	4.25E-10
bounding membrane of organelle	2.96E-08
lytic vacuole	8.15E-08
lysosomal lumen	1.13E-07
lytic vacuole membrane	1.22E-06

e

Group D (Downregulation)	
Pathways	
Term	adj. p-value
mRNA processing	3.84E-40
TNF-alpha NF-kB signaling pathway	7.10E-14
Cytoplasmic ribosomal proteins	1.09E-13
DNA replication	8.74E-12
Proteasome degradation	3.85E-10
Electron transport chain	1.11E-09
G1 to S cell cycle control	6.17E-09
Eukaryotic transcription initiation	4.39E-08
TCA cycle	6.4025E-05
Estrogen signaling	0.00026762
GO (Cellular Component)	
Term	adj. p-value
mRNA processing	4.09E-54
mRNA splicing, via spliceosome	5.60E-53
RNA splicing, via transesterification reactions with bulged adenosine as nucleophile	3.58E-50
gene expression	3.08E-46
cellular macromolecule biosynthetic process	2.85E-41

Supplementary Fig. 11. Characterization of the neck cell differentiation process in dataset 1. Related to Fig.2.

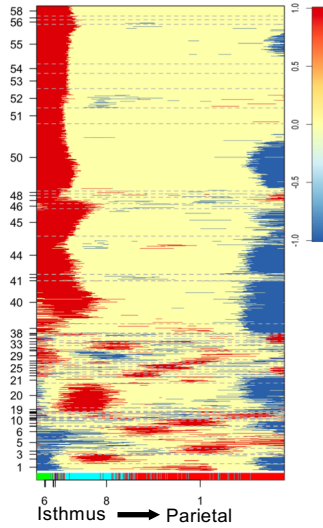
a Self-organizing map of binarized pseudotemporal expression profiles along the neck cell differentiation trajectory. The x-axis indicates the cells involved in the neck cell lineage that are colored according to cell types and the y-axis indicates the nodes.

b Hierarchical clustering of co-expression nodes in (b). The nodes in group C and D show upregulation and downregulation patterns of the genes in the neck cell differentiation trajectory, respectively. The x-axis indicates the cells involved in the neck cell lineage that are colored according to cell types and the y-axis indicates the nodes. The x-axis in (b) is not same as that of (a) because of the new hierarchical clustering of the cells. The colors for each cell type are shown on the right bottom corner.

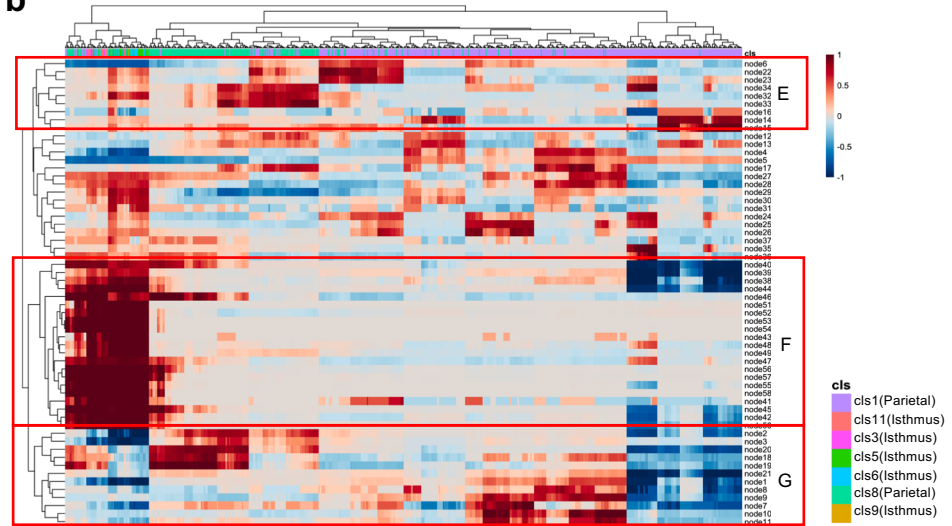
c Characteristics of group C and D identified in (b). Previously reported marker genes in each group are shown. Average pseudotemporal expression profile of the representative node is shown in gray line. The x-axis indicates pseudotime from isthmus progenitor cells to neck cells and the y-axis indicates expression level. Colors in each dot represent cell types, which corresponds to colors used in Supplementary Fig. 7a. Among the TFs involved in group C and D, the top 10 transcription factors specifically expressed in neck cells and isthmus progenitor cells ($\text{LogFC} > 0.25$) are shown, respectively.

d and e Characterization of the pseudotime-dependent genes included in group C (d) and group D (e). Upper panel, pathway enrichment analysis of the pseudotime-dependent genes. The four pathways and the top ten pathways with significant enrichment (adjusted p -value < 0.05) are listed in group C and D, respectively. Lower panel, GO analysis of the pseudotime-dependent genes. The top five terms with significant enrichment (adjusted p -value < 0.05) are listed. Adjusted p -value was determined using one-tailed Fisher's exact test with g:SCS method in g:Profiler³⁶ (pathways) and Fisher's exact test with Benjamini-Hochberg adjustment in Enrichr³⁷ (GO).

a Dataset 2 parietal cell lineage



b



c

	Marker gene	Expression pattern	TF
E	<i>Atp4b</i> <i>Kcnq1</i>	Node6 	
F	<i>Mki67</i> <i>Pcna</i> <i>Stmn1</i>	Node51 	<i>Cenpa</i> <i>Klf6</i> <i>Fos</i> <i>Dnmt1</i> <i>Fosb</i> <i>Tfdp1</i> <i>Atf3</i> <i>Foxq1</i> <i>Klf4</i> <i>Egr1</i>
G		Node20 	<i>Esrrg</i> <i>Chchd3</i> <i>Esrra</i> <i>Ybx2</i> <i>Mitf</i> <i>Nacc2</i> <i>Cxxc5</i> <i>Arhgap35</i> <i>Snopc5</i> <i>Mbnl2</i>

d

Group F (Downregulation)

Pathways

Term	adj. p-value
mRNA processing	3.60E-47
TNF-alpha NF-kB signaling pathway	1.75E-27
Estrogen signaling	5.50E-15
Cytoplasmic ribosomal proteins	2.63E-12
G1 to S cell cycle control	4.52E-12
EGFR1 signaling pathway	7.13E-12
Eukaryotic transcription initiation	1.46E-11
PluriNetWork: mechanisms associated with pluripotency	2.71E-10
DNA replication	3.17E-10
Translation factors	6.29E-09
Proteasome degradation	1.50E-07
IL-6 signaling pathway	0.0001212
FAS pathway and stress induction of HSP regulation	0.00016859
Wnt signaling pathway (NetPath)	0.00017451
Apoptosis	0.0004891
IL-7 signaling pathway	0.00052432
Delta-Notch signaling pathway	0.00139537
IL-5 signaling pathway	0.00390991
IL-3 signaling pathway	0.00496692
Toll-like receptor signaling	0.00849418

e

Group G (Transient upregulation)

Pathways

Term	adj. p-value
Electron transport chain	1.34E-45
Oxidative phosphorylation	1.41E-27
TCA cycle	3.41E-17
Fatty acid beta-oxidation	1.44E-09
Amino acid metabolism	1.17E-07
Glycolysis and gluconeogenesis	3.2851E-06
Mitochondrial long chain fatty acid beta-oxidation	5.642E-06
Fatty acid biosynthesis	0.01778986
Insulin signaling	0.0186317
Arachidonate epoxygenase / epoxide hydrolase	0.03885906

GO (Biological Pathway)

Term	adj. p-value
aerobic electron transport chain	7.30E-53
mitochondrial ATP synthesis coupled electron transport	2.63E-52
mitochondrial respiratory chain complex assembly	6.58E-37
mitochondrial electron transport, NADH to ubiquinone	3.64E-36
mitochondrial respiratory chain complex I assembly	2.68E-33

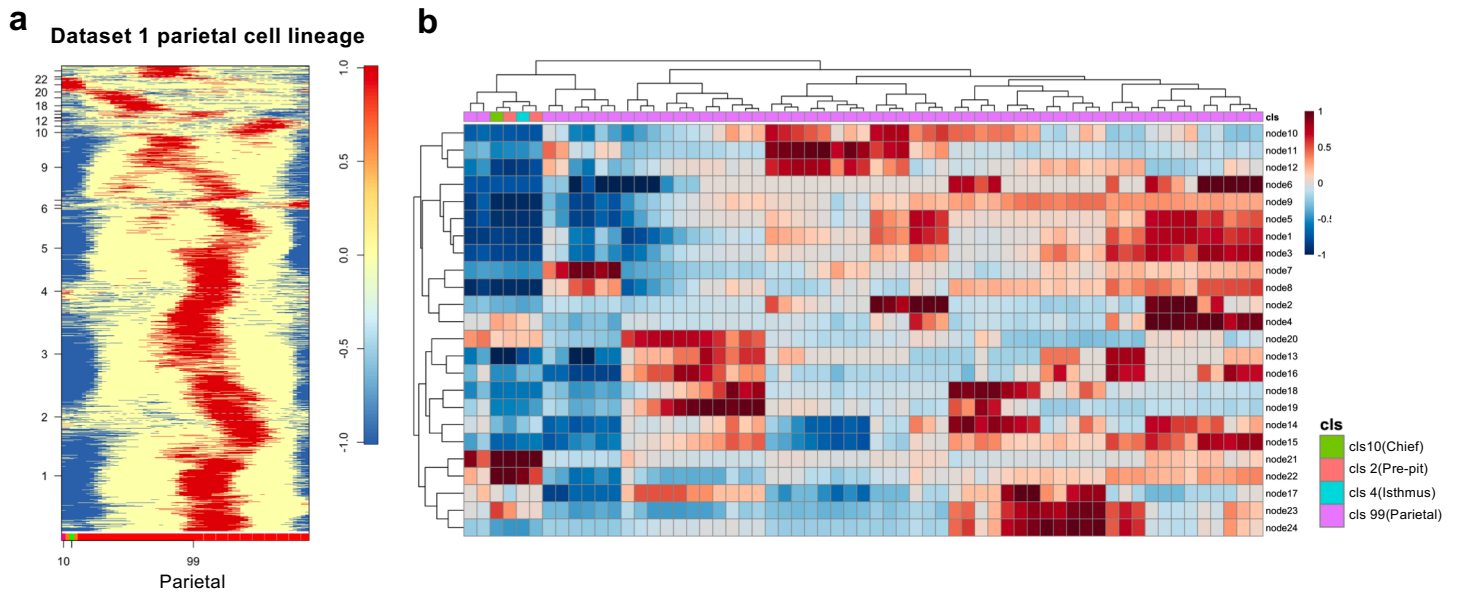
Supplementary Fig. 12. Characterization of the parietal cell differentiation process in dataset 2. Related to Fig.2.

a Self-organizing map of binarized pseudotemporal expression profiles along the parietal cell differentiation trajectory. The x-axis indicates the cells involved in the parietal cell lineage that are colored according to cell types and the y-axis indicates the nodes.

b Hierarchical clustering of co-expression nodes in (a). The nodes in group E, F, and G show upregulation, downregulation, and transient upregulation patterns of the genes in the parietal cell differentiation trajectory, respectively. The x-axis indicates the cells involved in the parietal cell lineage that are colored according to cell types and the y-axis indicates the nodes. The x-axis in (b) is not same as that of (a) because of the new hierarchical clustering of the cells. The colors for each cell type are shown on the right bottom corner.

c Characteristics of group E, F, and G identified in (b). Previously reported marker genes in each group are shown. Average pseudotemporal expression profile of the representative node is shown in black line. The x-axis indicates pseudotime from isthmus progenitor cells to parietal cells and the y-axis indicates expression level. Colors of each dot represent cell types, which corresponds to colors used in Fig. 2a. Among the TFs involved in group E, F, and G, the top 10 TFs specifically expressed in parietal cells and isthmus progenitor cells ($\text{LogFC} > 0.25$) are shown, respectively.

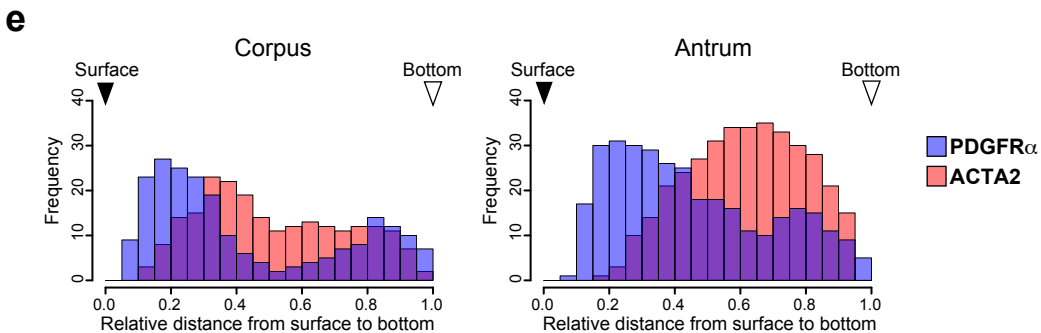
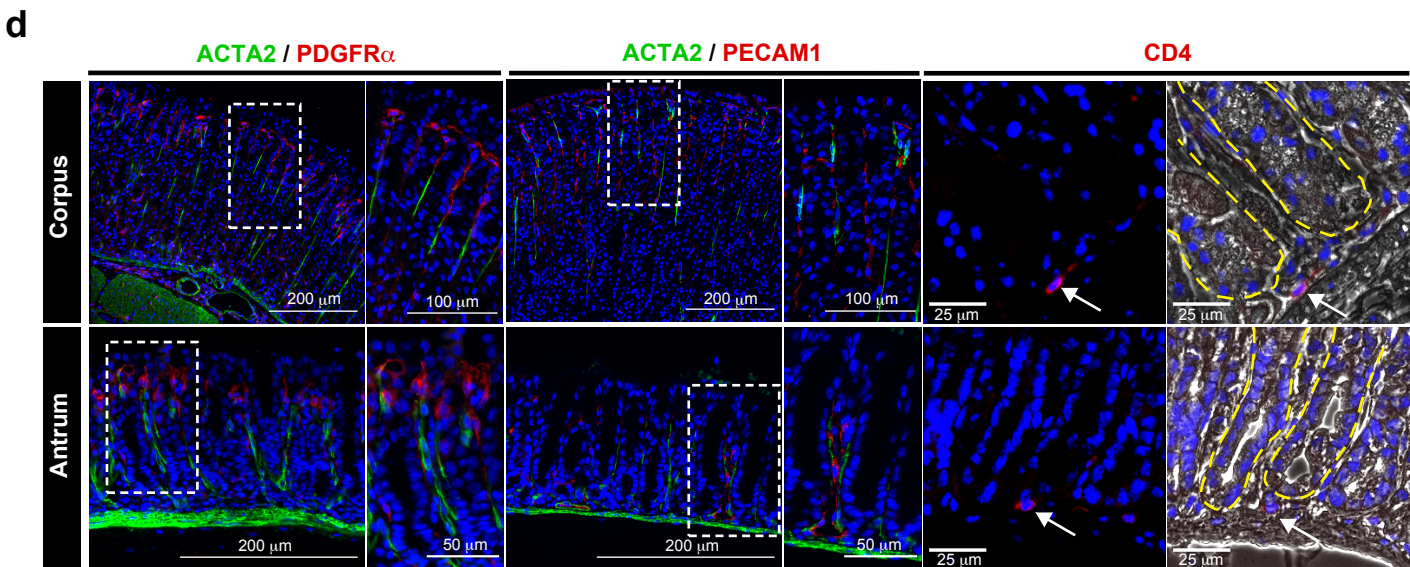
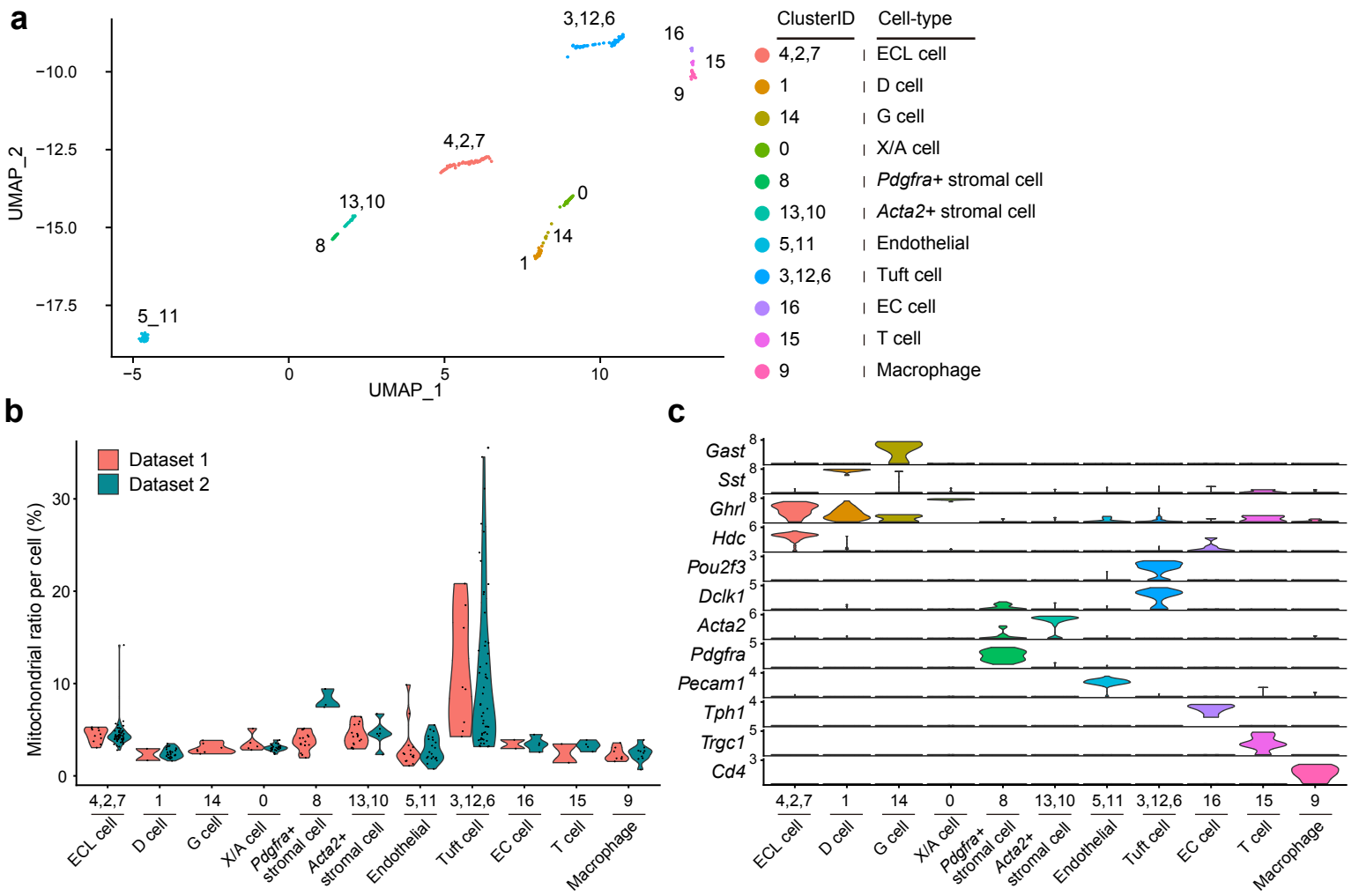
d and e Characterization of the pseudotime-dependent genes included in group F (d) and group G (e). Upper panel, pathway enrichment analysis of the pseudotime-dependent genes. The top 20 and the top 10 pathways with significant enrichment (adjusted p -value < 0.05) are listed in group F and G, respectively. Lower panel, GO analysis of the pseudotime-dependent genes. The top five terms with significant enrichment (adjusted p -value < 0.05) are listed. Adjusted p -value was determined using one-tailed Fisher's exact test with g:SCS method in g:Profiler³⁶ (pathways) and Fisher's exact test with Benjamini-Hochberg adjustment in Enrichr³⁷ (GO).



Supplementary Fig. 13. Characterization of the parietal cell differentiation process in dataset 1. Related to Fig.2.

a Self-organizing map of binarized pseudotemporal expression profiles along the parietal cell differentiation trajectory. The x-axis indicates the cells involved in the parietal cell lineage that are colored according to cell types and the y-axis indicates the nodes.

b Hierarchical clustering of co-expression nodes in (a). The x-axis indicates the cells involved in the parietal cell lineage that are colored according to cell types and the y-axis indicates the nodes. The x-axis in (b) is not same as that of (a) because of the new hierarchical clustering of the cells. The colors for each cell type are shown on the right bottom corner.



Supplementary Fig. 14. Characterization of gastric cells other than the major corpus epithelial cells. Related to Fig.3.

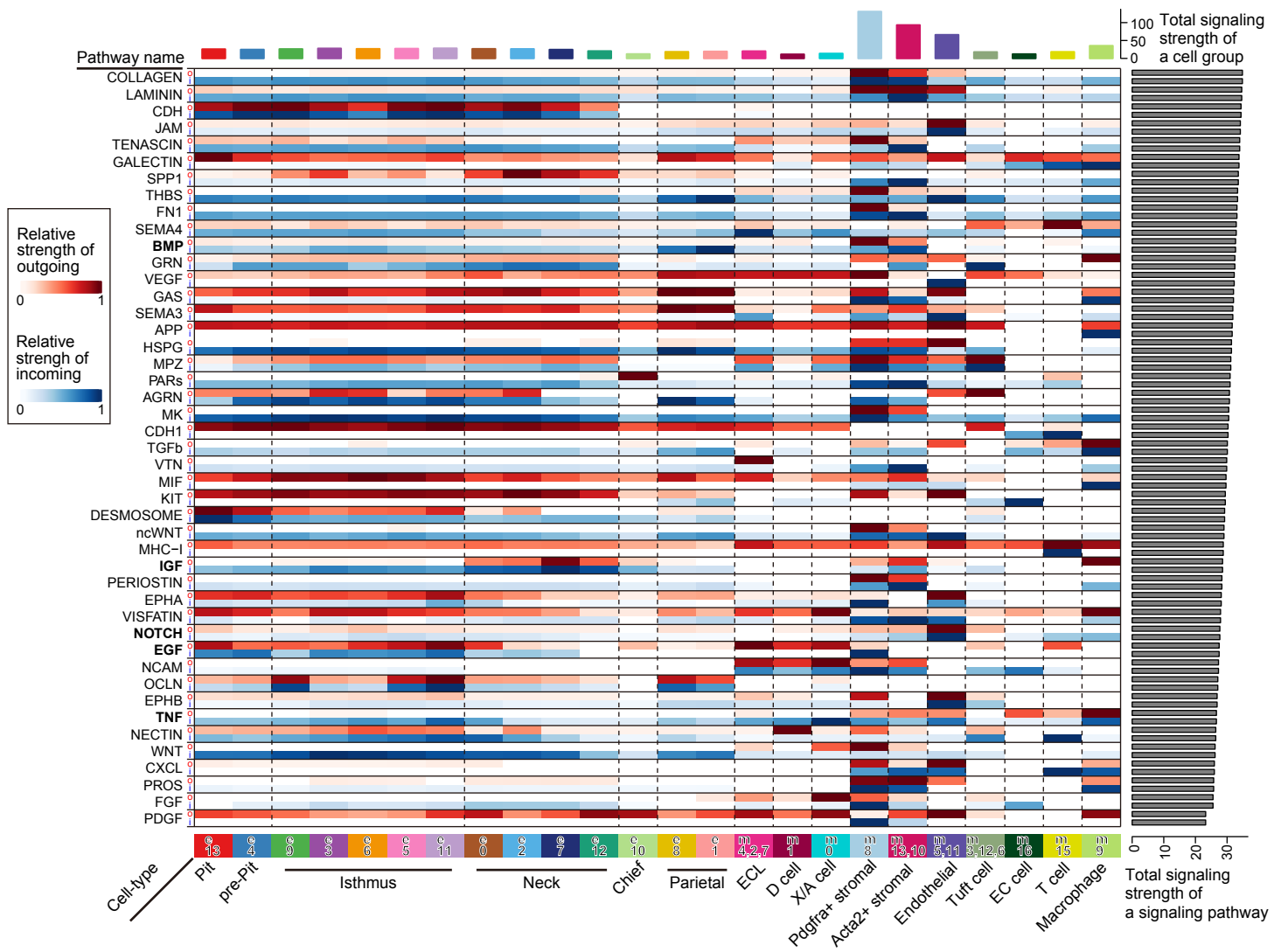
a UMAP visualization of gastric cells other than the major corpus epithelial identified in datasets 1 and 2.

b Violin plots showing mitochondrial ratio per cell in each cluster. The cells derived from datasets 1 and 2 are in red and green, respectively.

c Violin plots showing the expression of known marker genes in each cluster.

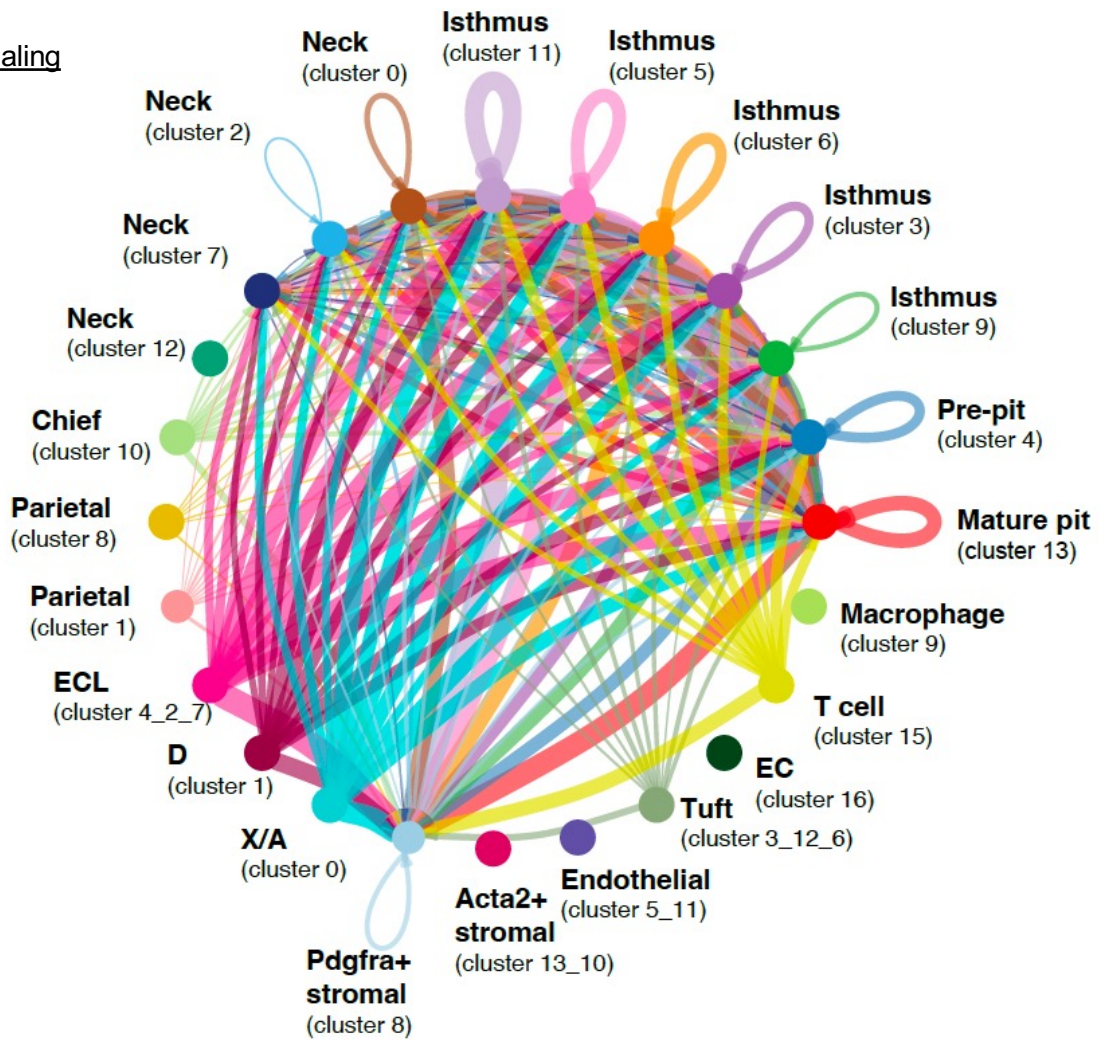
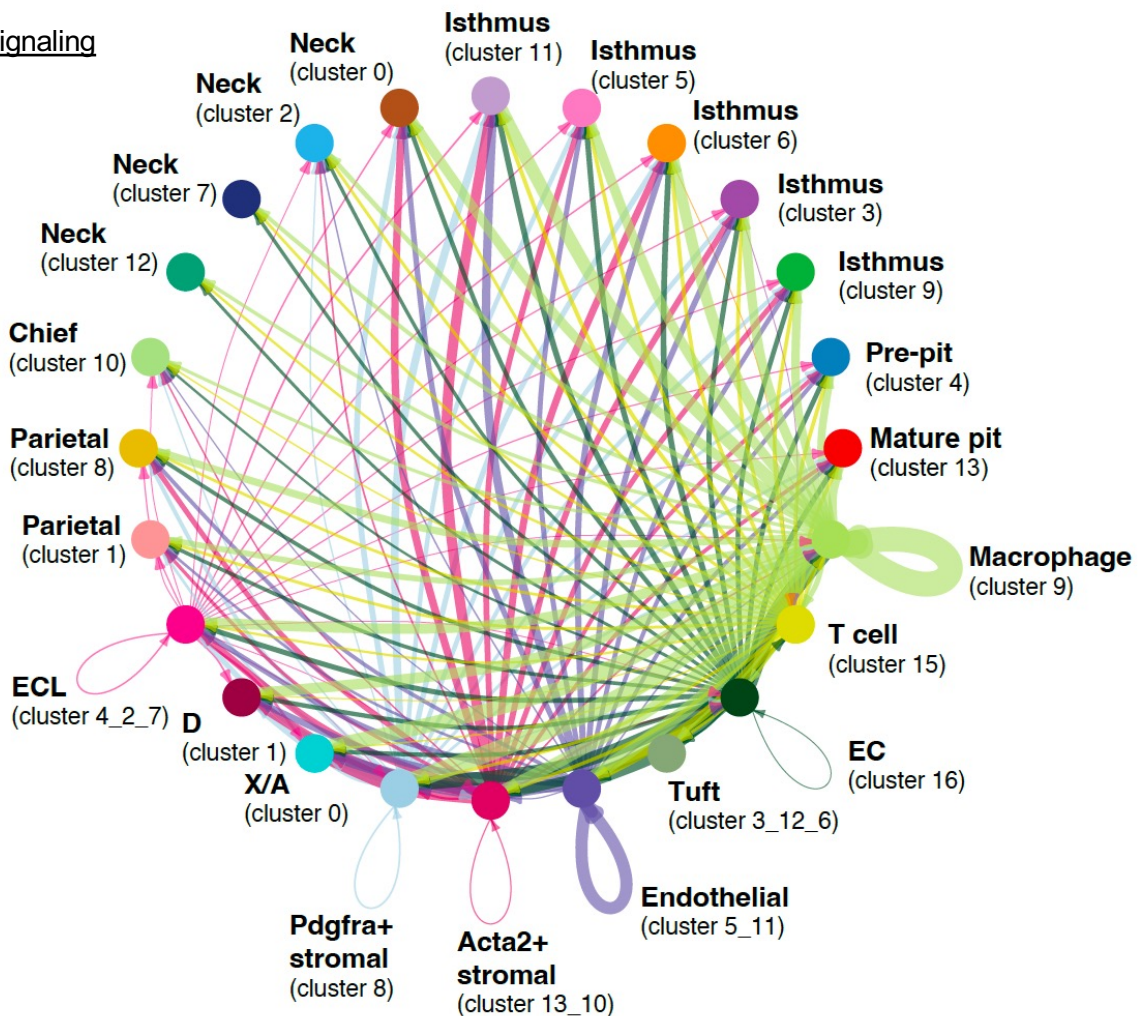
d Immunofluorescence staining of adult mouse corpus and antrum tissues with ACTA2 (green), PDGFR α (red), PECAM1 (red), CD4 (red), and DAPI (blue). High magnification images of the dotted squares are shown on the right side. As for CD4 staining, phase contrast pictures merged with CD4 and DAPI are shown on the right side. Yellowlines indicate each gastric gland. The images are representative of three independent experiments (ACTA2/PDGFR α) or two independent experiments (ACTA2/PECAM1 and CD4).

e Histogram showing the distribution of PDGFR α ⁺ (blue) and ACTA2⁺ (red) stromal cells in adult mouse corpus and antrum gastric units. The x-axis indicates the relative position in gastric glands, and the y-axis indicates the number of the stromal cells detected at each position.



Supplementary Fig. 15. CellChat-based Analysis of outgoing and incoming signaling in each cell type. Related to Fig. 3

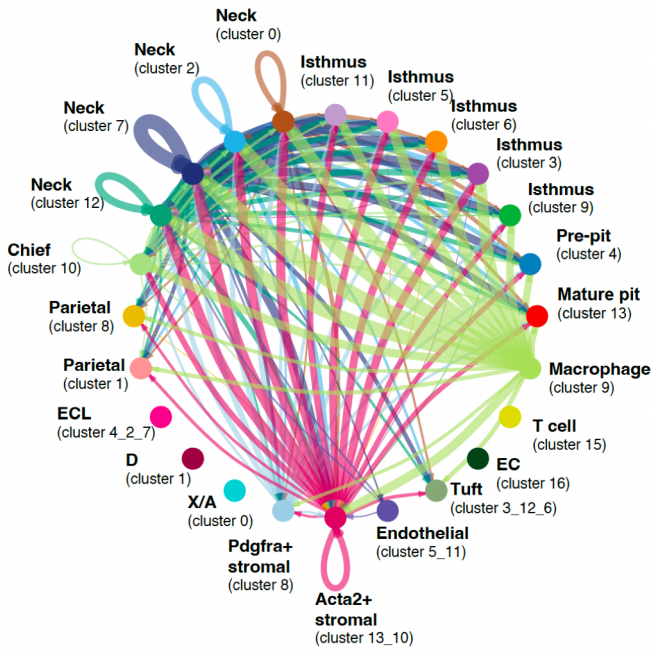
The x-axis indicates cell types and the y-axis indicates signaling pathways. For each signaling, the outgoing signal intensity is shown in red (upper row) and the incoming signal intensity is shown in blue (lower row).

aEGF signaling**b**TNF signaling

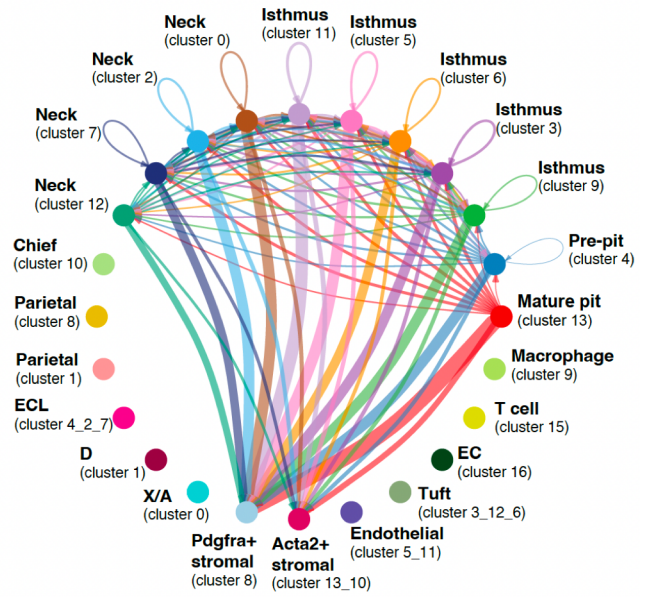
Supplementary Fig. 16. Signaling networks inferred by CellChat analysis. Related to Fig.3.

CellChat analysis predicted cell-cell communication among all gastric cell types for EGF (a), and TNF (b) signaling pathways. Line width represents communication probabilities.

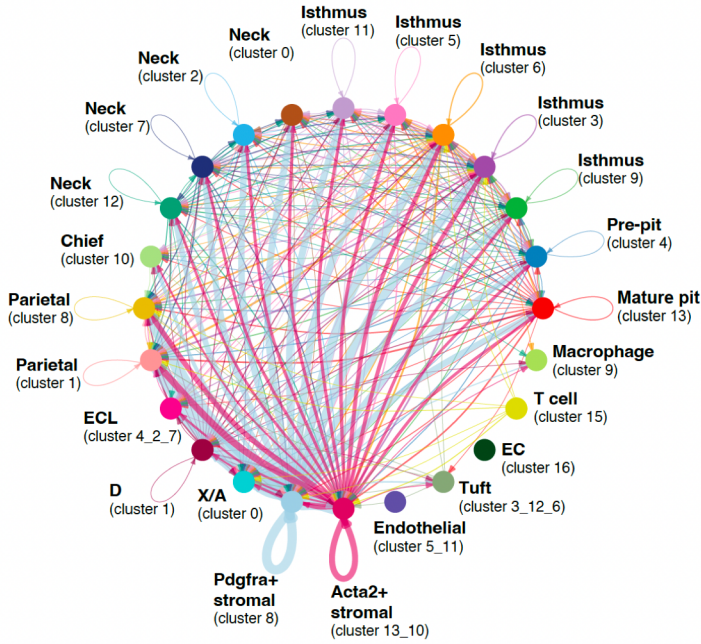
a IGF signaling network



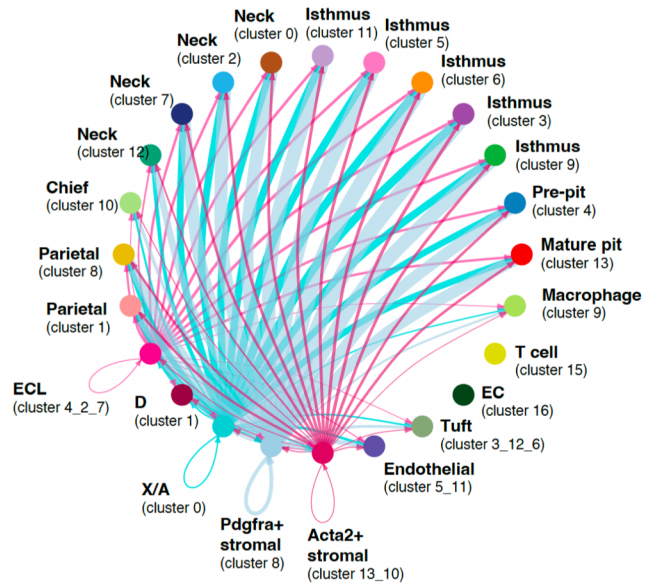
b SHH signaling network



c BMP signaling network

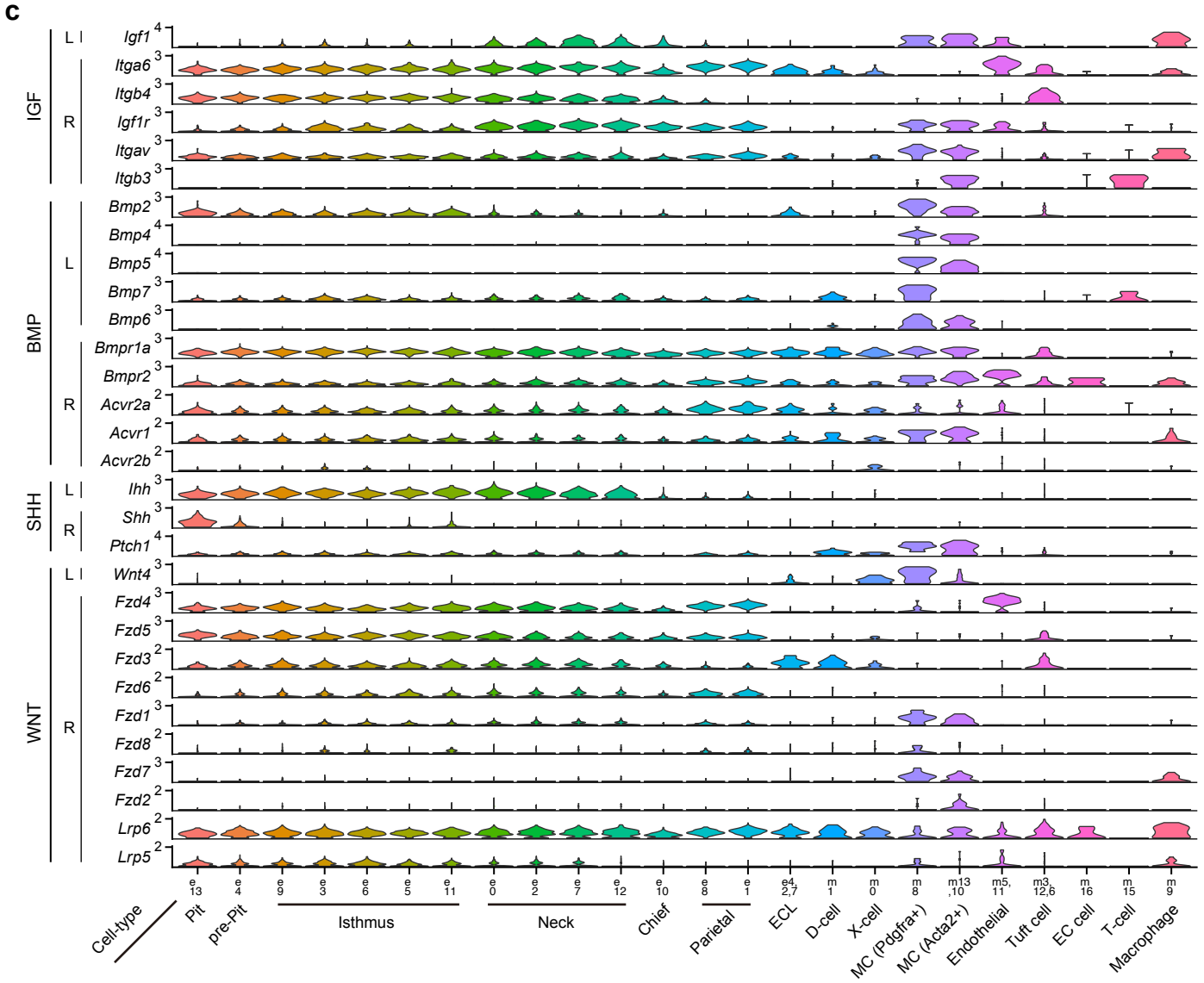
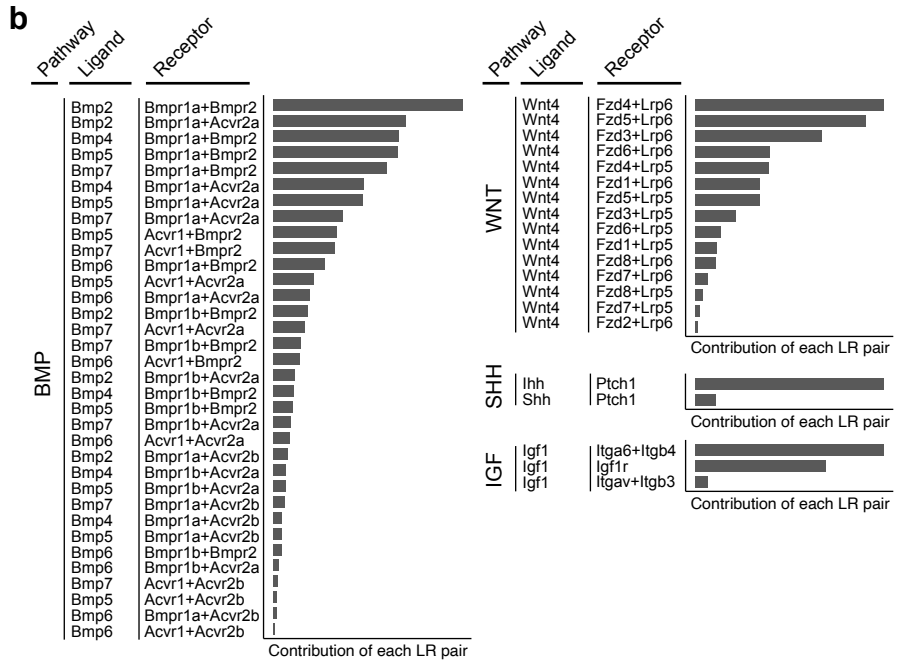
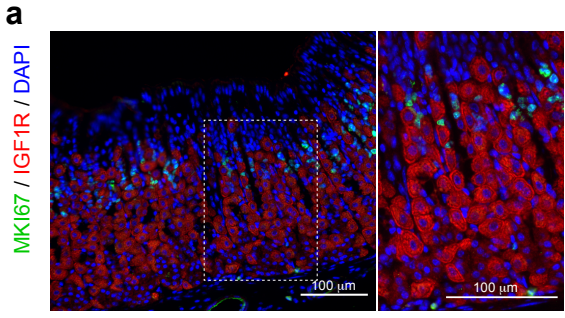


d WNT signaling network



Supplementary Fig. 17. Signaling networks inferred by CellChat analysis. Related to Fig.3.

CellChat analysis predicted cell-cell communication among all gastric cell types for IGF (a), SHH (b), BMP (c), and WNT (d) signaling pathways. Line width represents communication probabilities.

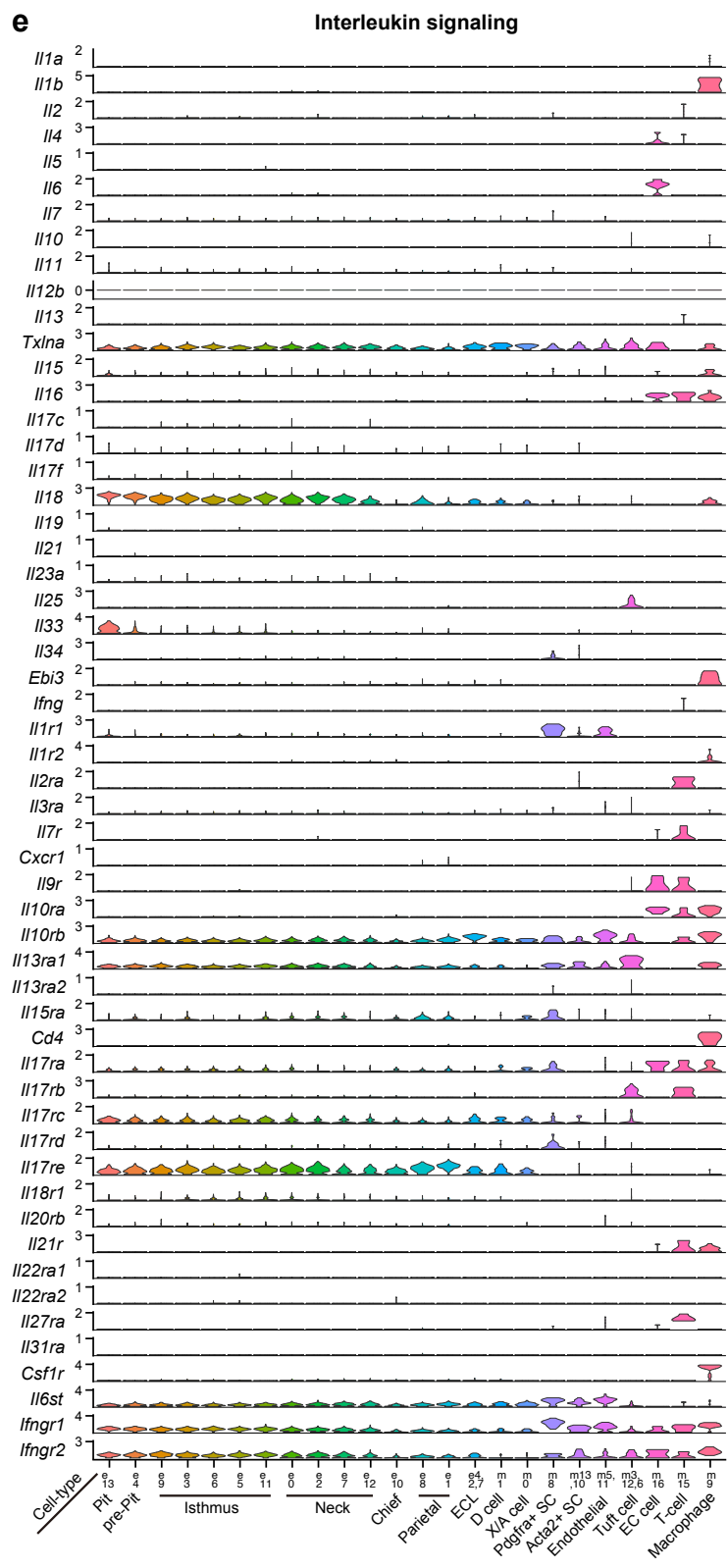
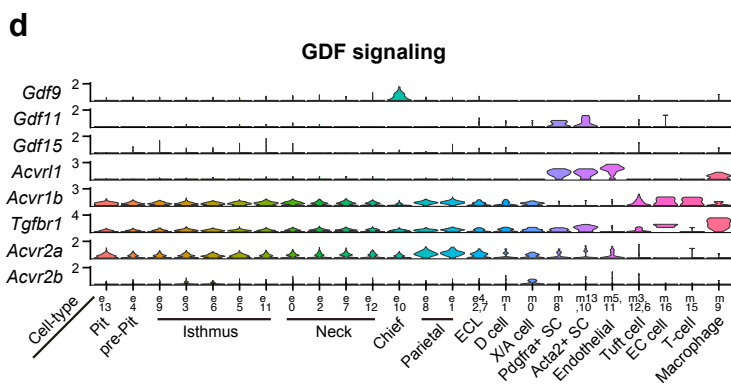
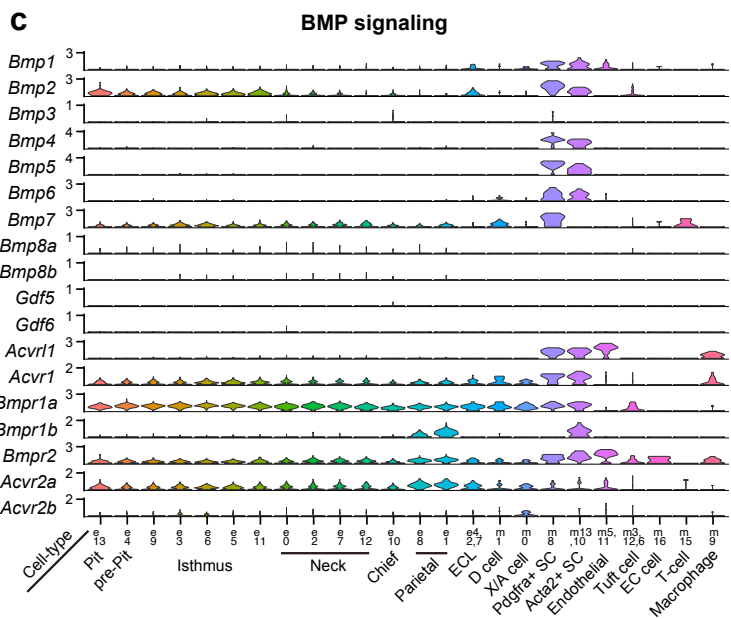
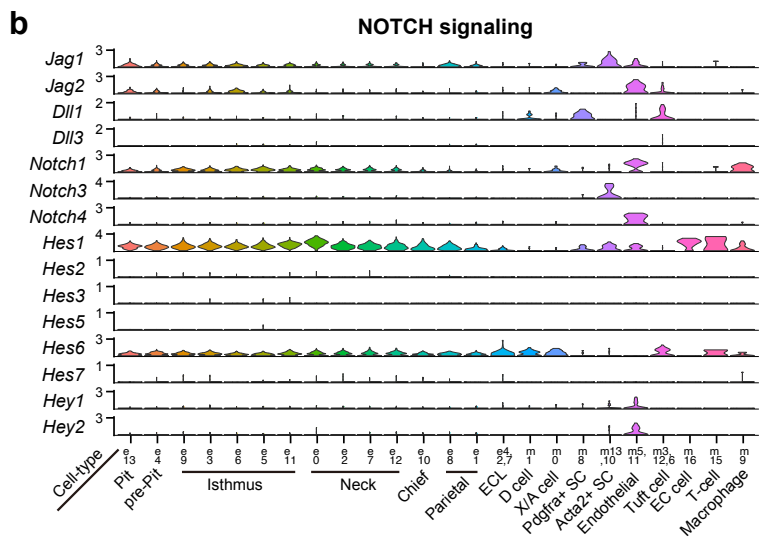
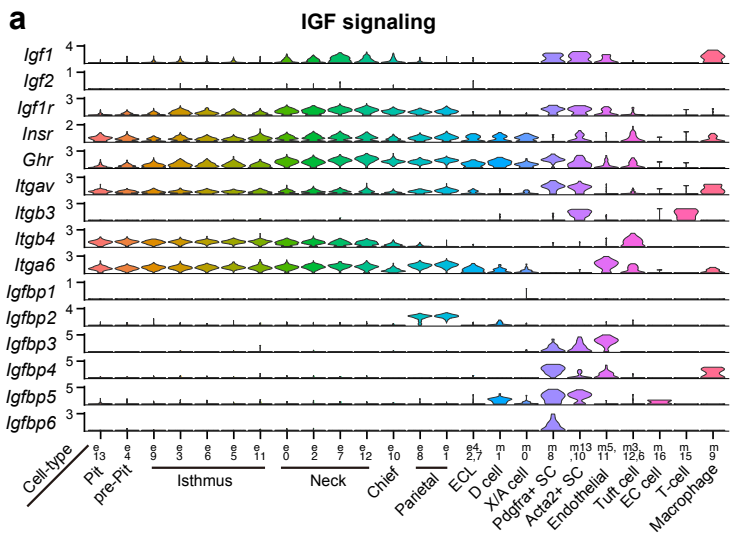


Supplementary Fig. 18. Expression pattern of major inferred ligand-receptor pairs for each signaling pathway.

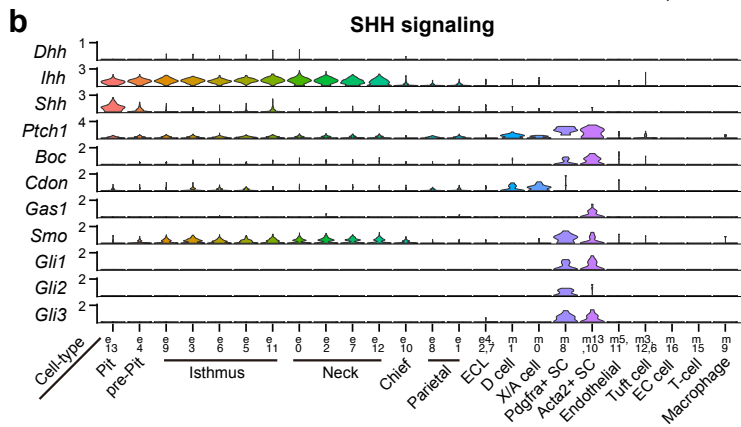
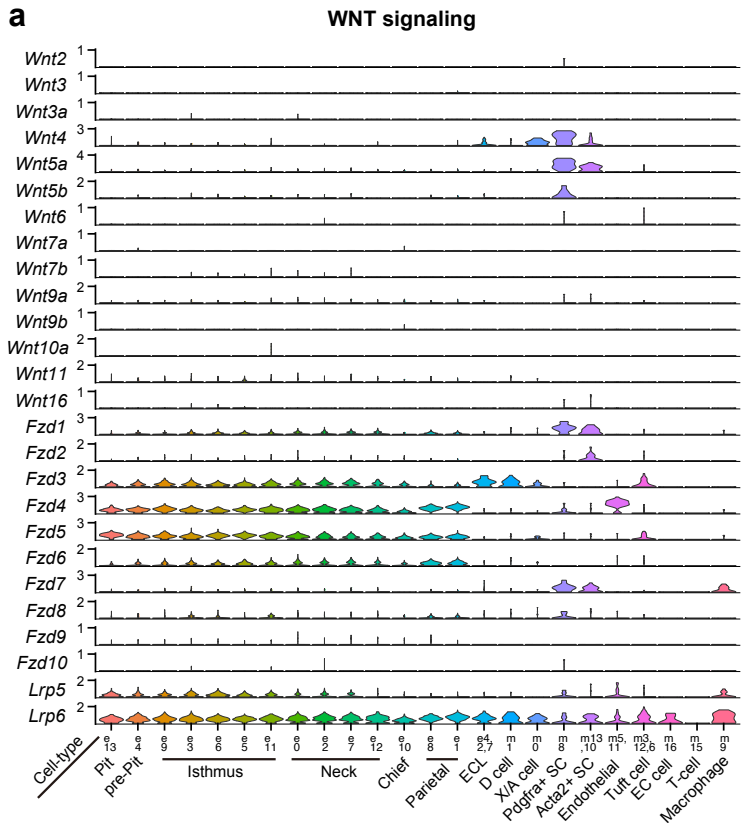
a Immunofluorescence staining of MKI67 (green), IGF1R (red), and DAPI (blue) in adult mouse corpus tissues. High magnification images of the dotted squares are shown on the right side. The images are representative of two independent experiments.

b Relative contribution of BMP, WNT, SHH, and IGF ligand-receptor pairs calculated by CellChat.

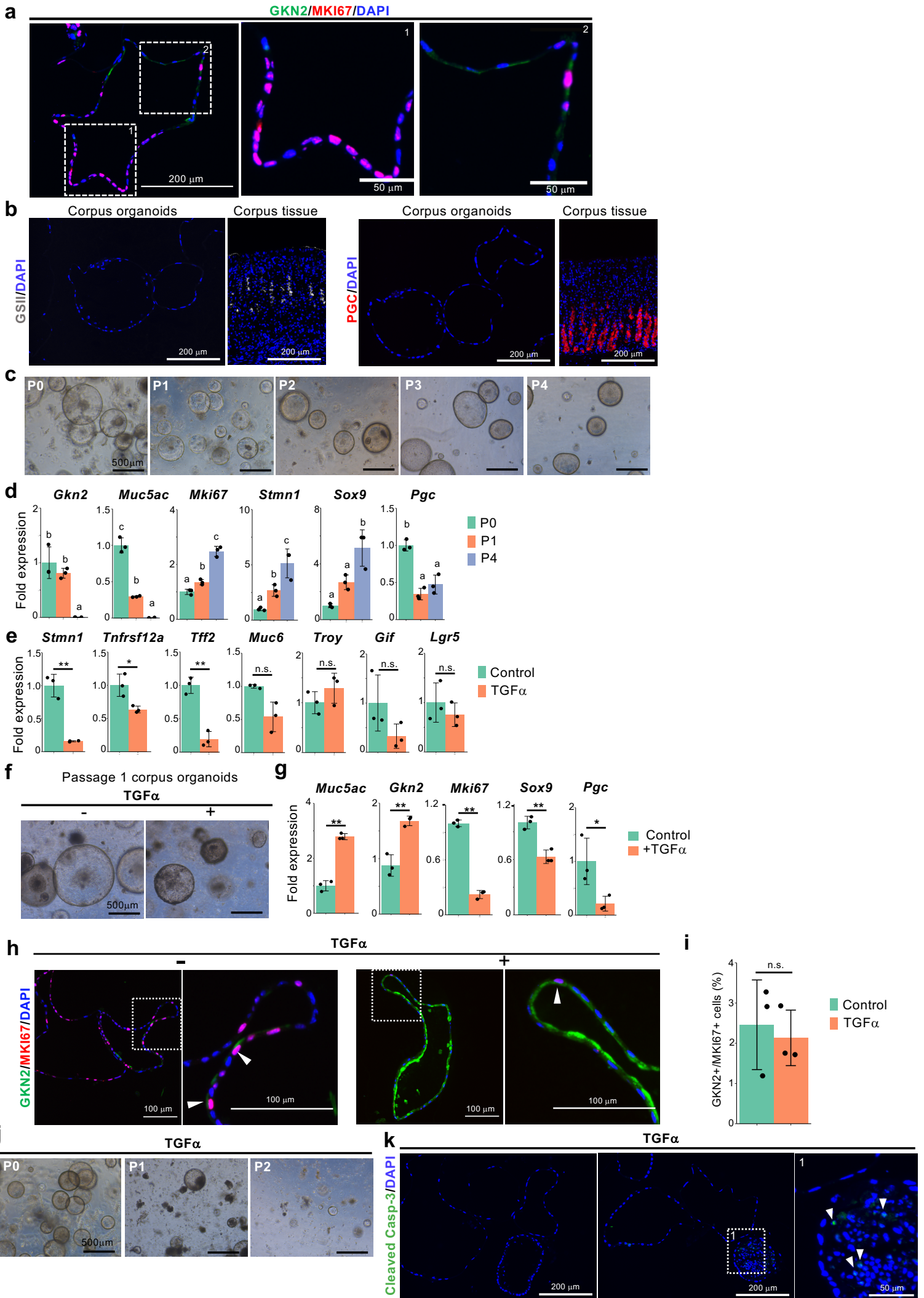
c Violin plots showing the expression of IGF, BMP, SHH, and WNT ligands and receptors that were identified as major contributors by CellChat.



Supplementary Fig. 19. Expression pattern of ligands, receptors, and downstream regulators for IGF (a), NOTCH (b), BMP (c), GDF (d), and Interleukin (e) signaling pathways across all gastric cell types.



Supplementary Fig. 20. Expression pattern of ligands and receptors for WNT (a) and SHH (b) signaling pathway across all gastric cell types.



Supplementary Fig. 21. TGF α promotes pit cell differentiation and suppresses cell proliferation. Related to Fig. 4.

a Immunofluorescence staining of GKN2 (green), MKI67 (red), and DAPI (blue) in corpus organoids prepared from adult mouse corpus. MKI67⁻ cells frequently express low level of GKN2. High magnification images of the dotted squares are shown on the right side.

b Immunofluorescence staining of GSII (white), PGC (red), and DAPI (blue) in corpus organoids and adult corpus tissue. The images are representative of two independent experiments.

c Corpus organoids cultured in the control medium at passage 0–4. Scale bar, 500 μ m.

d qPCR analysis of gastric epithelial cell marker expression in the corpus organoids at passage 0, 1, and 4 in (c). Data are presented as mean fold changes \pm SD ($n = 3$ biologically independent samples). P1 vs P0 *n.s.*, P4 vs P0 $p = 0.0010$, P4 vs P1 $p = 0.0032$ for *Gkn2*; $p < 0.0001$, $p < 0.0001$, $p = 0.0025$ for *Muc5ac*; $p = 0.0400$, $p < 0.0001$, $p = 0.0001$ for *Mki67*; $p = 0.0334$, $p < 0.0001$, $p = 0.0003$ for *Stmn1*; *n.s.*, $p = 0.0020$, $p = 0.0240$ for *Sox9*; $p = 0.0004$, $p = 0.0013$, *n.s.* for *Pgc*.

e qPCR analysis of gastric epithelial cell marker expression in the organoids in Fig. 4a. Data are presented as mean fold changes \pm SD ($n = 3$ biologically independent samples for each culture condition). ** $p = 0.0011$ for *Stmn1*; * $p = 0.0230$ for *Tnfrsf12a*; ** $p = 0.0011$ for *Tff2*.

f Passage 1 corpus organoids treated with or without TGF α . The organoids were grown without TGF α for 6 days and then dissociated with a recombinant enzyme, TrypLE Express, to generate passage 1 organoids. The passage 1 organoids were further grown with or without TGF α (25 ng/mL) for 6 days. Scale bar, 500 μ m.

g qPCR analysis of gastric epithelial marker expression in corpus organoids in (f). Data are presented as mean fold changes \pm SD ($n = 3$ biologically independent samples for each culture condition). ** $p = 0.0001$ for *Muc5ac*; ** $p = 0.0027$ for *Gkn2*; ** $p < 0.0001$ for *Mki67*; ** $p = 0.0029$ for *Sox9*; * $p = 0.0397$ for *Pgc*.

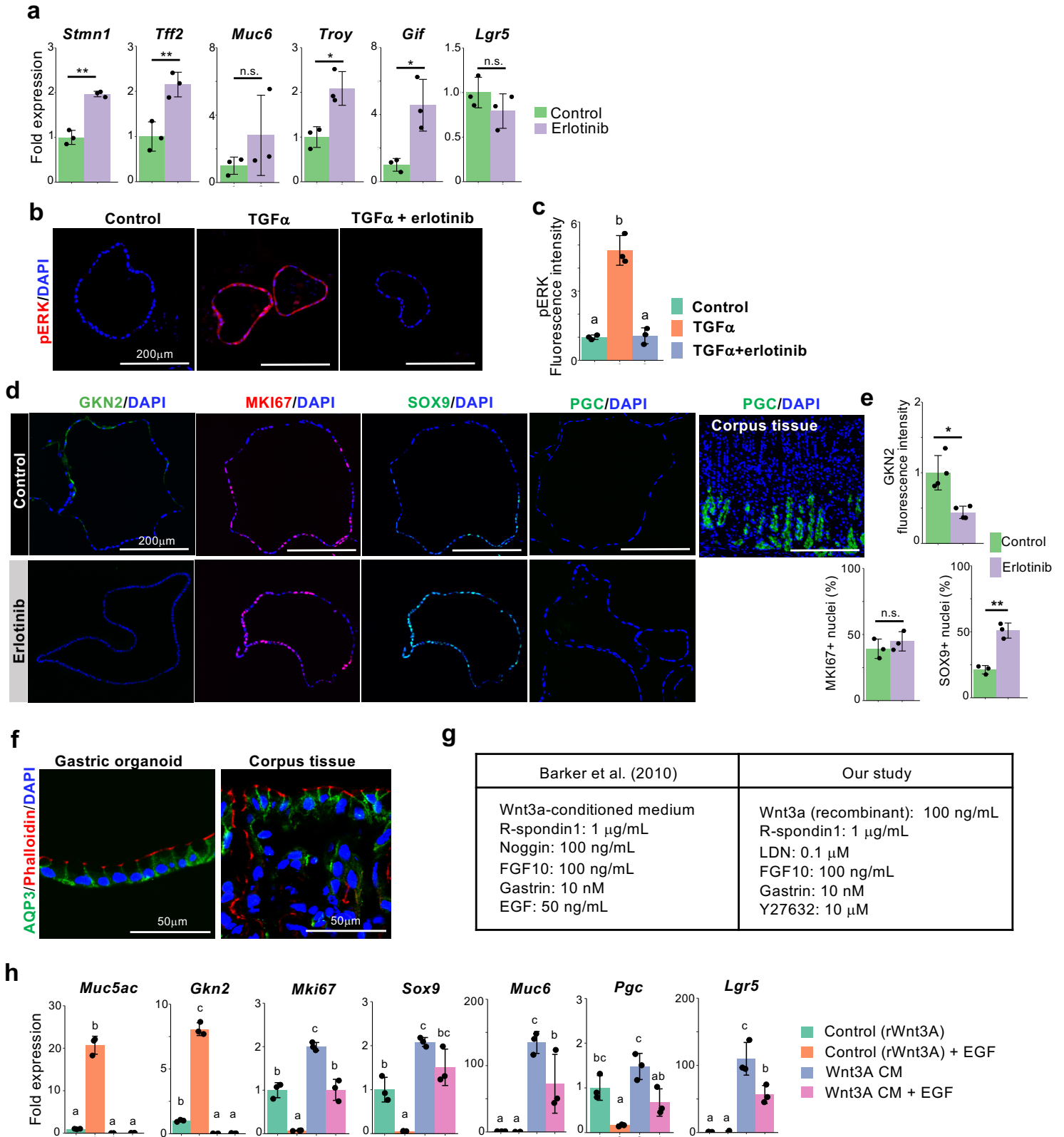
h Double immunofluorescence staining of GKN2 (green) and MKI67 (red) in corpus organoids treated with or without TGF α (12.5 ng/mL) for 6 days. Arrowheads indicate GKN2⁺/MKI67⁺ cells. Insets show high magnification images of boxed areas.

i Quantification of GKN2⁺/MKI67⁺ cells in corpus organoids in (h). Data are presented as mean fold changes \pm SD ($n = 3$ biologically independent samples for each culture condition).

j Gastric organoids treated with TGF α (12.5 ng/mL) from the beginning of the culture at passage 0, 1, and 2. The number of organoids was dramatically decreased after first passage. Scale bar, 500 μ m. The images are representative of two independent experiments.

k Immunofluorescence staining of cleaved caspase-3 (green) with nuclear DAPI staining (blue) in corpus organoids treated with TGF α (12.5 ng/mL) for 6 days. Arrowheads indicate cleaved caspase-3⁺ shed cells in the lumen. High magnification images of the dotted squares are shown on the right side. The images are representative of two independent experiments.

Statistical information: significance was calculated by two-tailed Student's *t*-tests for samples with equal variances or two-sided Welch's *t*-tests for samples with unequal variances in (e, g, and i) (* $p < 0.05$; ** $p < 0.01$); significance was calculated by one-way ANOVA followed by Tukey post hoc test at the 0.05 significance level in (d). Source data are provided as a Source Data file.



Supplementary Fig. 22. Inhibition of EGFR signaling suppresses pit cell differentiation. Related to Fig. 4.

a qPCR analysis of gastric epithelial cell marker expression in erlotinib-treated corpus organoids in Fig. 4f. Data are presented as mean fold changes \pm SD ($n = 3$ biologically independent samples for each culture condition). ** $p = 0.0005$ for *Stmn1*; ** $p = 0.0093$ for *Tff2*; * $p = 0.0131$ for *Troy*; * $p = 0.0179$ for *Gif*.

b Immunofluorescence analysis of pERK (red) and DAPI (blue) in corpus organoids cultured with or without TGF α and erlotinib. Scale bar, 200 μ m.

c Quantification of pERK fluorescence intensity in corpus organoids in (b). Data are presented as mean fold changes \pm SD ($n = 3$ biologically independent samples). Each data point represents the mean value of at least ten organoids. TGF α vs Control $p < 0.0001$, TGF α + erlotinib vs Control *n.s.*, TGF α + erlotinib vs TGF α $p < 0.0001$.

d Immunofluorescence staining of GKN2 (green), MKI67 (red), SOX9 (green), PGC (green), and DAPI (blue) in corpus organoids treated with or without erlotinib (0.5 μ M). The adult mouse corpus tissues stained with PGC (green) is shown in the upper right corner as a positive control. Scale bar, 200 μ m.

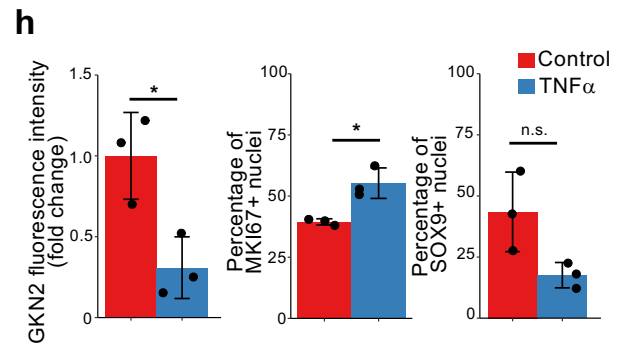
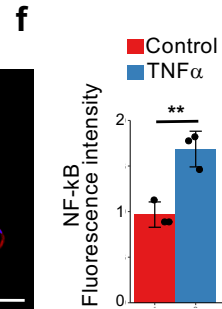
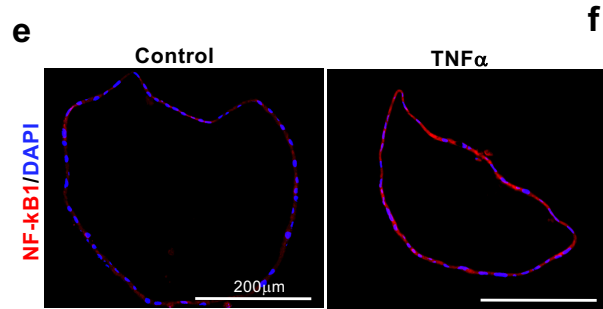
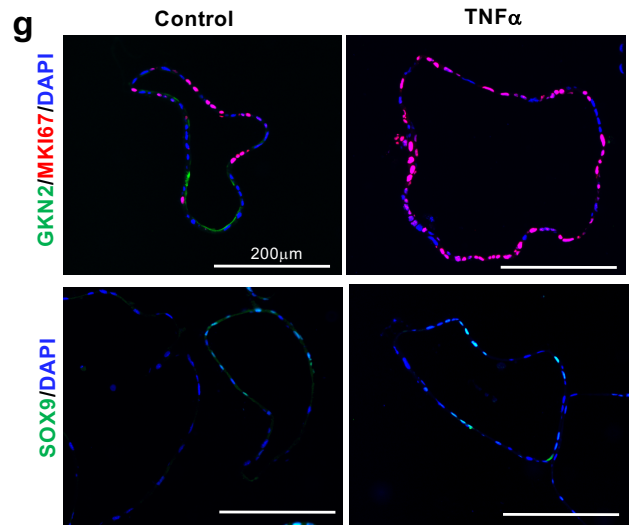
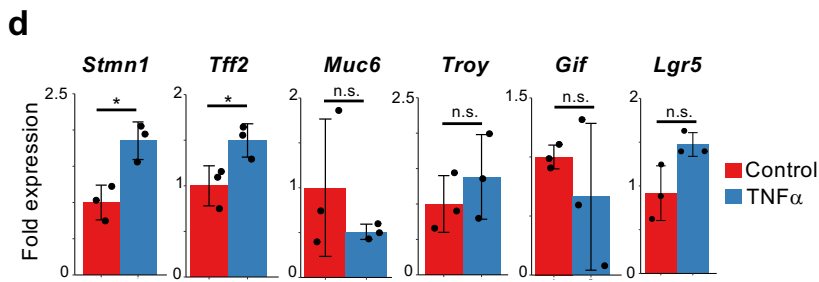
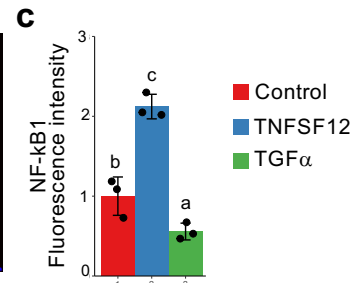
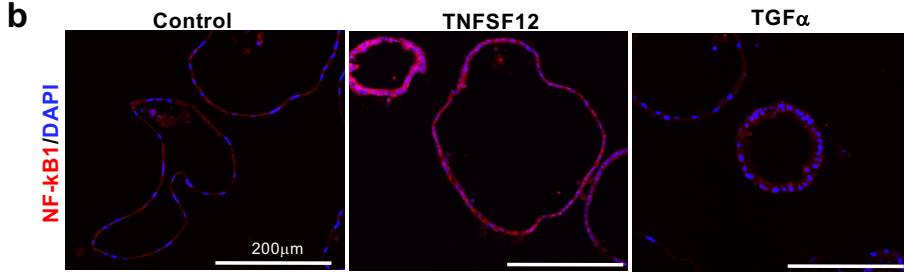
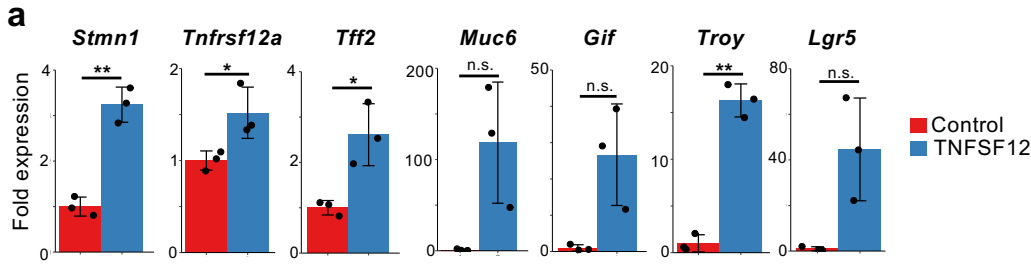
e Quantification of GKN2 fluorescence intensity and the percentage of MKI67⁺ and SOX9⁺ cells in the corpus organoids in (d). Data are presented as mean fold changes \pm SD ($n = 3$ or 4 biologically independent samples). ** $p = 0.0049$ for GKN2 fluorescence intensity; ** $p = 0.0014$ for SOX9⁺ nuclei.

f The corpus organoid and the corpus tissue stained with anti-AQP3 antibody (green), phalloidin (red), and DAPI (blue). Images were captured by laser confocal microscopy and representative of three independent experiments.

g Comparison of growth factors and chemicals used in the previous study (Barker et al. 2010) and those used in our study.

h qPCR analysis of gastric epithelial cell marker expression in the corpus organoids cultured with rWnt3a (100 ng/mL) or Wnt3a CM. The response to EGF (50 ng/mL) was analyzed. Data are presented as mean fold changes \pm SD ($n = 3$ biologically independent samples for each culture condition). Control + EGF vs Control $p < 0.001$, WNT3A CM vs Control *n.s.*, WNT3A CM + EGF vs Control *n.s.*, WNT3A CM vs Control + EGF $p < 0.0001$, WNT3A CM + EGF vs Control + EGF $p < 0.0001$, WNT3A CM + EGF vs WNT3A CM *n.s.* for *Muc5ac*; $p < 0.0001$, $p = 0.0060$, $p = 0.0066$, $p < 0.0001$, $p < 0.0001$, *n.s.* for *Gkn2*; $p = 0.0004$, $p = 0.0002$, *n.s.*, $p < 0.0001$, $p = 0.0003$, $p = 0.0002$ for *Mki67*; $p = 0.0082$, $p = 0.0037$, *n.s.*, $p < 0.0001$, $p = 0.0005$, *n.s.* for *Sox9*; *n.s.*, $p = 0.0006$, $p = 0.02486$, $p = 0.0005$, $p = 0.0235$, $p = 0.0486$ for *Muc6*; $p = 0.01548$, *n.s.*, *n.s.*, $p = 0.0010$, *n.s.*, $p = 0.0191$ for *Pgc*; *n.s.*, $p < 0.0001$, $p = 0.0053$, $p < 0.0001$, $p = 0.0053$, $p = 0.0069$ for *Lgr5*.

Statistical information: significance was calculated by two-tailed Student's *t*-tests for samples with equal variances or two-sided Welch's *t*-tests for samples with unequal variances in (a) and (e) (* $p < 0.05$; ** $p < 0.01$); significance was calculated by one-way ANOVA followed by Tukey post hoc test at the 0.05 significance level in (c) and (h). Source data are provided as a Source Data file.



Supplementary Fig. 23. Activation of NF-κB signaling suppresses pit cell differentiation. Related to Fig. 5.

a qPCR analysis of gastric epithelial cell markers in the corpus gastric organoids cultured with or without 100 ng/mL TNFSF12 in Fig. 5a. Data are presented as mean fold changes \pm SD ($n = 3$ biologically independent samples for each culture condition). ** $p = 0.0009$ for *Stmn1*; * $p = 0.0390$ for *Tnfrsf12a*; * $p = 0.0164$ for *Tff2*; ** $p = 0.0009$ for *Troy*.

b Immunofluorescence analysis of NF-κB1 (red) and DAPI (blue) in the corpus gastric organoids cultured with or without 100 ng/mL TNFSF12 and 12.5 ng/mL TGF α . Scale bar, 200 μ m.

c Quantification of the fluorescence intensity of NF-κB1 in the corpus organoids in (b). Data are presented as mean fold changes \pm SD ($n = 3$ biologically independent samples). Each data point represents the mean value of at least ten organoids. TGF α vs Control $p = 0.0485$, TNFSF12 vs Control $p = 0.0006$, TNFSF12 vs TGF α $p < 0.0001$.

d qPCR analysis of gastric epithelial cell markers in corpus gastric organoids cultured with or without 100 ng/mL TNF α in Fig. 5e. Data are presented as mean fold changes \pm SD ($n = 3$ biologically independent samples for each culture condition). * $p = 0.0139$ for *Stmn1*; * $p = 0.0393$ for *Tff2*.

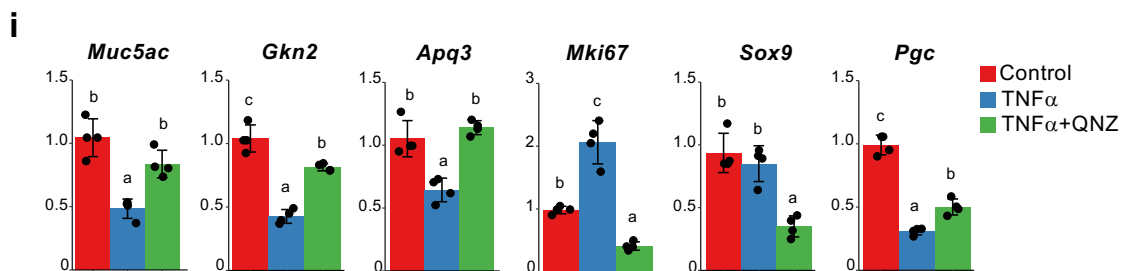
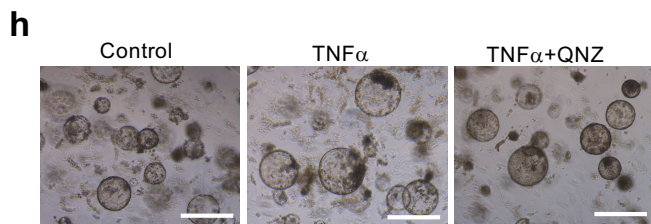
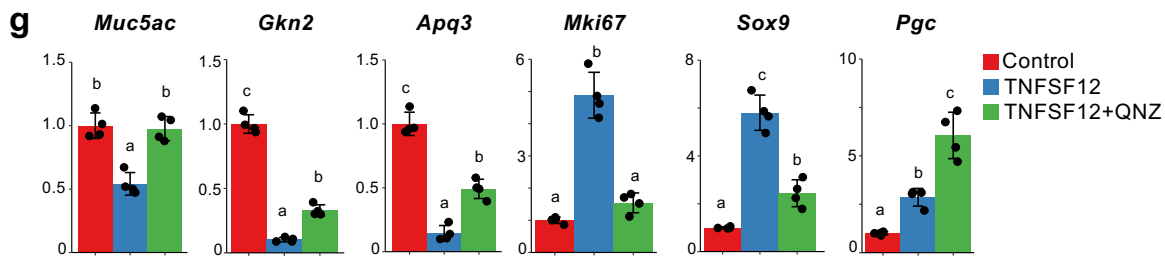
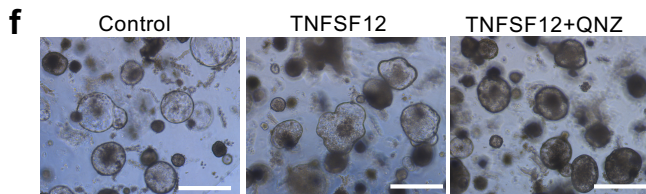
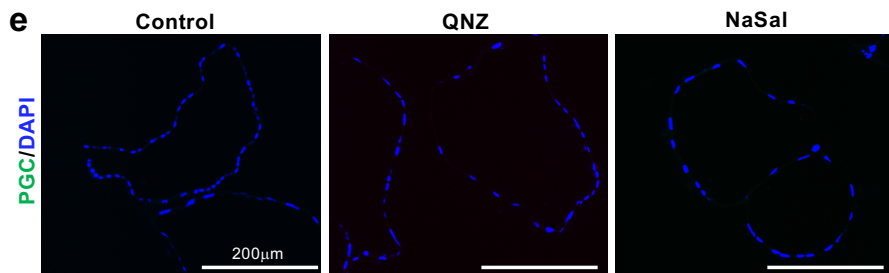
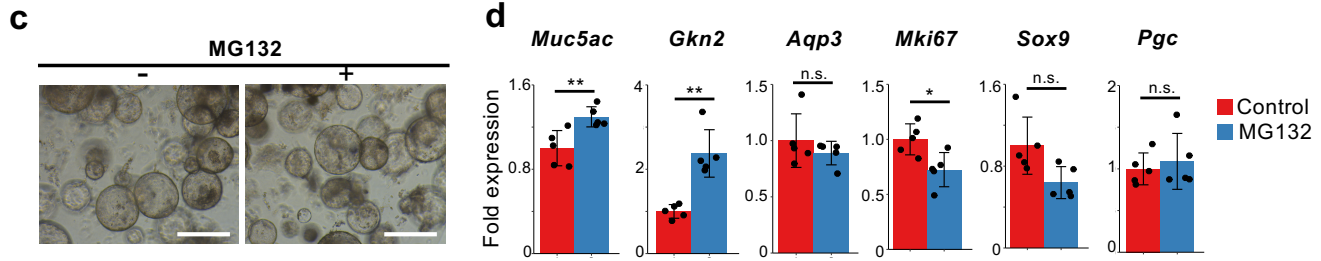
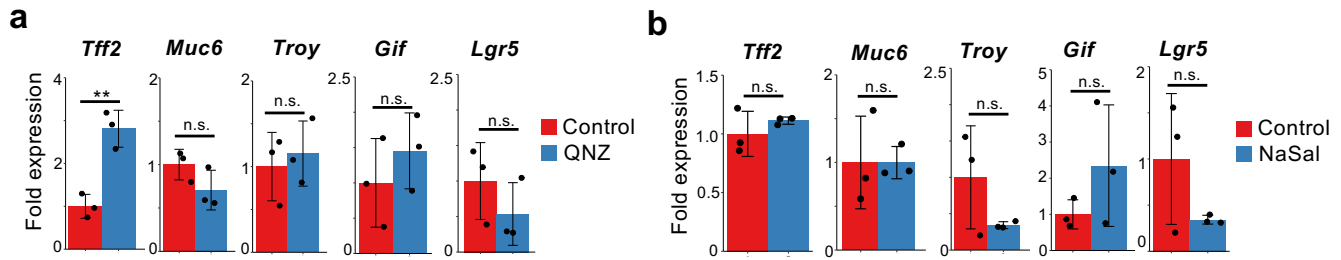
e Immunofluorescence staining of NF-κB1 (red) and DAPI (blue) in the corpus gastric organoids cultured with or without 100 ng/mL TNF α . Scale bar, 200 μ m.

f Quantification of the fluorescence intensity of NF-κB1 in the gastric organoids in (e). Data are presented as mean fold changes \pm SD ($n = 3$ biologically independent samples). Each data point represents the mean value of ten organoids. ** $p = 0.0066$.

g Immunofluorescence staining of GKN2 (green), MKI67 (red), SOX9 (green), and DAPI (blue) in the corpus gastric organoids cultured with or without 100 ng/mL TNF α . Scale bar, 200 μ m.

h Quantification of GKN2 fluorescence intensity and the percentage of MKI67⁺ and SOX9⁺ cells of the corpus gastric organoids in (g). Data are presented as mean fold changes \pm SD ($n = 3$ biologically independent samples). Each data point represents the mean value of at least ten organoids. * $p = 0.0220$ for GKN2 fluorescence intensity, * $p = 0.0126$ for MKI67⁺ nuclei.

Statistical information: significance was calculated by two-tailed Student's *t*-tests for samples with equal variances or two-sided Welch's *t*-tests for samples with unequal variances in (a), (d), (f), and (h) (* $p < 0.05$; ** $p < 0.01$); significance was calculated by one-way ANOVA followed by Tukey post hoc test at the 0.05 significance level in (c). Source data are provided as a Source Data file.



Supplementary Fig. 24. Inhibition of NF- κ B signaling induces pit cell differentiation. Related to Fig. 6.

a qPCR analysis of gastric epithelial cell markers in corpus gastric organoids cultured with or without a NF- κ B inhibitor, QNZ (16 nM) in Fig. 6a. Data are presented as mean fold changes \pm SD ($n = 3$ biologically independent samples). ** $p = 0.0036$ for *Tff2*.

b qPCR analysis of gastric epithelial cell marker expression in corpus gastric organoids cultured with or without a NF- κ B inhibitor NaSal (1.25 mM) in Fig. 6c. Data are presented as mean fold changes \pm SD ($n = 3$ biologically independent samples).

c Corpus organoids cultured with or without a proteasome inhibitor, MG132 (3 μ M). Scale bar, 500 μ m.

d qPCR analysis of gastric epithelial cell marker expression in the gastric organoids in (c). Data are presented as mean fold changes \pm SD ($n = 5$ biologically independent samples). ** $p = 0.0086$ for *Muc5ac*, ** $p = 0.0041$ for *Gkn2*, * $p = 0.0189$ for *Mki67*.

e Immunofluorescence staining of PGC (green) and DAPI (blue) in the corpus gastric organoids cultured with or without 16 nM QNZ or 1.25 mM NaSal. Scale bar, 200 μ m. The images are representative of two biologically independent samples.

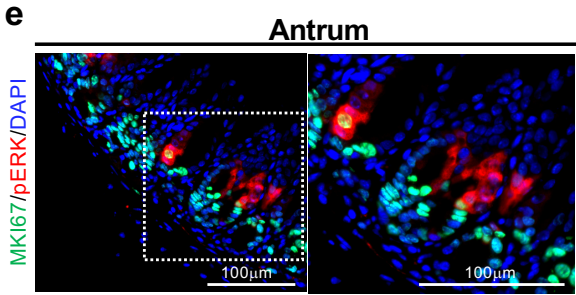
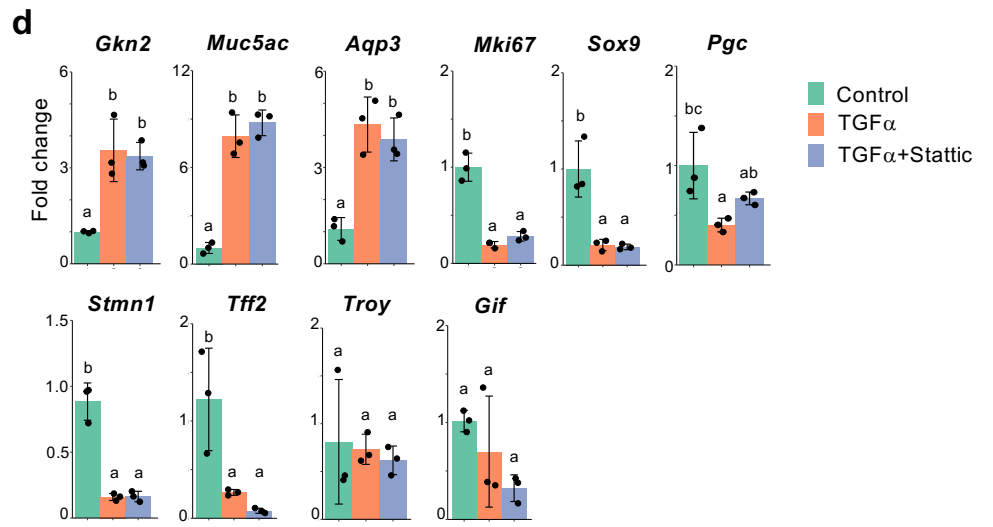
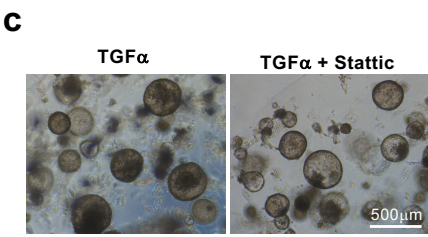
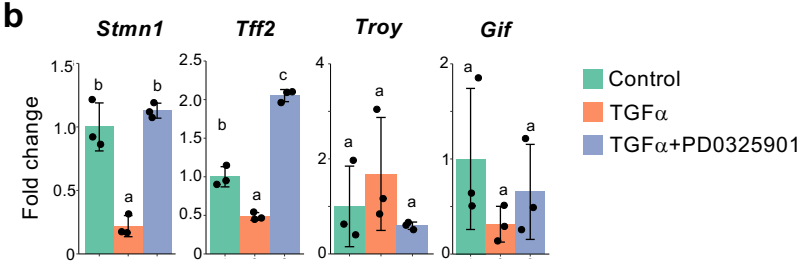
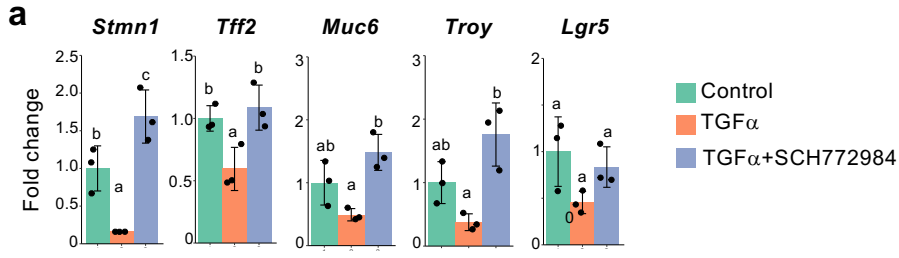
f Corpus organoids cultured with or without TNFSF12 (100 ng/mL) and a NF- κ B inhibitor QNZ (80 nM). Scale bar, 500 μ m.

g qPCR analysis of gastric epithelial cell marker expression in the corpus organoids in (f). Data are presented as mean fold changes \pm SD ($n = 4$ biologically independent samples). TNFSF12 vs Control $p = 0.0002$, TNFSF12 + QNZ vs Control *n.s.*, TNFSF12 + QNZ vs TNFSF12 $p = 0.0003$ for *Muc5ac*; $p < 0.0001$, $p < 0.0001$, $p = 0.0003$ for *Gkn2*; $p < 0.0001$, $p < 0.0001$, $p = 0.0003$ for *Aqp3*; $p < 0.0001$, *n.s.*, $p < 0.0001$ for *Mki67*; $p < 0.0001$, $p = 0.0106$, $p < 0.0001$ for *Sox9*; $p = 0.0154$, $p < 0.0001$, $p = 0.0005$ for *Pgc*.

h Corpus organoids cultured with or without TNFa (100 ng/mL) and a NF- κ B inhibitor QNZ (80 nM). Scale bar, 500 μ m.

i qPCR analysis of gastric epithelial cell marker expression in the corpus organoids in (h). Data are presented as mean fold changes \pm SD ($n = 4$ biologically independent samples). TNFa vs Control $p = 0.0002$, TNFa + QNZ vs Control $p = 0.0733$, TNFa + QNZ vs TNFa $p = 0.0049$ for *Muc5ac*; $p < 0.0001$, $p = 0.0038$, $p < 0.0001$ for *Gkn2*; $p = 0.0009$, *n.s.*, $p = 0.0002$ for *Aqp3*; $p = 0.0001$, $p = 0.0085$, $p < 0.0001$ for *Mki67*; *n.s.*, $p = 0.0004$, $p = 0.0012$ for *Sox9*; $p < 0.0001$, $p < 0.0001$, $p = 0.0036$ for *Pgc*.

Statistical information: significance was calculated by two-tailed Student's *t*-tests for samples with equal variances or two-sided Welch's *t*-tests for samples with unequal variances in (a), (b), (d). * $p < 0.05$; ** $p < 0.01$. In (g) and (i), significance was calculated by one-way ANOVA followed by Tukey post hoc test (significance level, $p < 0.05$). Source data are provided as a Source Data file.



Supplementary Fig. 25. Activation of ERK pathway is required for pit cell differentiation. Related to Fig. 7

a qPCR analysis of gastric epithelial cell markers in corpus organoids cultured with or without TGF α (12.5 ng/mL) and an ERK1/2 inhibitor, SCH772984 (0.4 μ M). Data are presented as mean fold changes \pm SD ($n = 3$ biologically independent samples). TGF α vs Control $p = 0.0197$, TGF α + SCH vs Control $p = 0.0449$, TGF α + SCH vs TGF α $p = 0.0010$ for *Stmn1*; $p = 0.0437$, *n.s.*, $p = 0.0196$ for *Tff2*; *n.s.*, *n.s.*, $p = 0.0072$ for *Troy*; *n.s.*, *n.s.*, *n.s.* for *Lgr5*.

b qPCR analysis of gastric epithelial cell markers in corpus organoids cultured with or without TGF α (12.5 ng/mL) and a MEK inhibitor PD0325901 (1 μ M). Data are presented as mean fold changes \pm SD ($n = 3$ biologically independent samples). TGF α vs Control $p = 0.0006$, TGF α + PD03 vs Control *n.s.*, TGF α + PD03 vs TGF α $p = 0.0002$ for *Stmn1*; $p = 0.0012$, $p < 0.0001$, $p < 0.0001$ for *Tff2*; *n.s.*, *n.s.*, *n.s.*, for *Troy*; *n.s.*, *n.s.*, *n.s.*, for *Gif*.

c Corpus organoids treated with or without a Stat3 inhibitor Stattic. The organoids were cultured in the presence of TGF α (12.5 ng/mL) with or without Stattic (50 μ M) for 6 days. Scale bar, 500 μ m.

d qPCR analysis of gastric epithelial cell marker expression in the corpus organoids in (c). Data are presented as mean fold changes \pm SD ($n = 3$ biologically independent samples for each culture condition). Note that Stattic did not affect the expression of pit cell markers and *Mki67*. TGF α vs Control $p = 0.0055$, TGF α + Stattic vs Control $p = 0.0079$, TGF α + Stattic vs TGF α *n.s.* for *Gkn2*; $p = 0.0002$, $p = 0.0001$, *n.s.* for *Muc5ac*; $p = 0.0027$, $p = 0.0047$, *n.s.* for *Aqp3*; $p < 0.0001$, $p = 0.0001$, *n.s.* for *Mki67*; $p = 0.0033$, $p = 0.0029$, *n.s.* for *Sox9*; $p = 0.0248$, *n.s.*, *n.s.* for *Pgc*; $p = 0.0001$, $p = 0.0001$, *n.s.* for *Stmn1*; $p = 0.0200$, $p = 0.0088$, *n.s.* for *Tff2*; *n.s.*, *n.s.*, *n.s.* for *Troy*; *n.s.*, *n.s.*, *n.s.* for *Gif*.

e Immunofluorescence staining of pERK (red), MKI67 (green), and DAPI (blue) in the mouse antrum tissue. Inset shows the high magnification image of boxed area. The image are a representative of three independent experiments.

Statistical information: significance was calculated by one-way ANOVA followed by Tukey post hoc test in (a), (b), and (d) (significance level, $p < 0.05$).

<i>b-actin</i>	F	GGCTGTATTCCCCTCCATCG
	R	CCAGTTGGTAACAATGCCATGT
<i>Muc5ac</i>	F	CAGGACTCTCTGAAATCGTACCA
	R	AAGGCTCGTACCACAGGGA
<i>Gkn2</i>	F	ATGAAACCCCTCGTGGCATT
	R	TGTCTCCTGGATATTGCCTCC
<i>Aqp3</i>	F	GCTTTTGGCTTCGCTGTCAC
	R	TAGATGGGCAGCTTGATCCAG
<i>Mki67</i>	F	ATCATTGACCGCTCCTTTAGGT
	R	GCTCGCCTTGATGGTTCCT
<i>Sox9</i>	F	AGTACCCGCATCTGCACAAC
	R	ACGAAGGGTCTCTTCTCGCT
<i>Pgc</i>	F	CCACCTACTACACTCAAGGGC
	R	AACTCCTGGTTAGGGACCTGG
<i>Stmn1</i>	F	TCTGTCCCCGATTTCCTCC
	R	AGCTGCTTCAAGACTTCCGC
<i>Tnfrsf12a</i>	F	GTGTTGGGATTTCGGCTTGGT
	R	GTCCATGCACTTGTCGAGGTC
<i>Tff2</i>	F	TGCTCTGGTAGAGGGCGAG
	R	CGACGCTAGAGTCAAAGCAG
<i>Muc6</i>	F	CGGCTGCGTCTGTCCTAAG
	R	GCATAGTCACATGGGCATTCT
<i>Gif</i>	F	CCCTCTACCTCCTAAGTGTTCTC
	R	CTGAGTCAGTCACCGAGTTCT
<i>Troy</i>	F	GACTGCCTGCCAGGATTTTAC
	R	CAGTGTGGTTCGTAGGGAGG
<i>Lgr5</i>	F	CCTACTCGAAGACTTACCCAGT
	R	GCATTGGGGTGAATGATAGCA

Supplementary Table 1. List of the primers used in this study.